BROOKHAVEN
NATIONAL LABORATORY

BNL-114156-2017-JA

The Phenology of Leaf Quality and its Within-Canopy Variation are Essential for Accurate Modeling of Photosynthesis in Tropical Evergreen Forests

J. Wu

Accepted for publication in Global Change Biology

May 2017

Environmental & Climate Science Dept.

Brookhaven National Laboratory

U.S. Department of Energy
USDOE Office of Science (SC),
Biological and Environmental Research (BER) (SC-23)

DISCLAIMER

The phenology of leaf quality and its within-canopy variation are essential for accurate modeling of photosynthesis in tropical evergreen forests

Running Head: Modeling tropical photosynthetic seasonality

Authors
Jin Wu[1*], Shawn P. Serbin[1], Xiangtao Xu[2], Loren P. Albert[3], Min Chen[4,5], Ran Meng[1], Scott R. Saleska[3], Alistair Rogers[1]

Institute or laboratory of origin
[1] Environmental & Climate Sciences Department, Brookhaven National Laboratory, Upton, New York, NY, 11973
[2] Department of Geosciences, Princeton University, Princeton, NJ, 08544
[3] Department of Ecology and Evolutionary Biology, University of Arizona, Tucson, AZ, 85721
[4] Department of Global Ecology, Carnegie Institution for Science, Stanford, CA, 94305
[5] Joint Global Change Research Institute, Pacific Northwest National Laboratory, College Park, MD, 20740

* Corresponding author: 631-344 3361; jinwu@bnl.gov

Key words: big leaf; sun/shade; multi-layer; light use efficiency; gross primary productivity; leaf age; leaf area index; photosynthetic capacity

Type of Paper: Original Research

Abstract:

Leaf quantity (i.e. canopy leaf area index, LAI), quality (i.e. per-area photosynthetic capacity), and longevity all influence the photosynthetic seasonality of tropical evergreen forests. However, these components of tropical leaf phenology are poorly represented in most terrestrial biosphere models (TBMs). Here, we explored alternative options for the representation of leaf phenology effects in TBMs that employ the Farquahar, von Caemmerer & Berry (FvCB) representation of CO_2 assimilation. We developed a two-fraction leaf (sun and shade), two-layer canopy (upper and lower) photosynthesis model to evaluate different modeling approaches and assessed three components of phenological variations (i.e. leaf quantity, quality, and within-canopy variation in leaf longevity). Our model was driven by the prescribed seasonality of leaf quantity and quality derived from ground based measurements within an Amazonian evergreen forest. Modeled photosynthetic seasonality was not sensitive to leaf quantity, but was highly sensitive to leaf quality and its vertical distribution within the canopy, with markedly more sensitivity to upper canopy leaf quality. This is because light absorption in tropical canopies is near maximal for the entire year, implying that seasonal changes in LAI have little impact on total canopy light absorption; and because leaf quality has a greater effect on photosynthesis of sunlit leaves than light limited, shade leaves and sunlit foliage are more abundant in the upper canopy. Our two-fraction leaf, two-layer canopy model which accounted for all three phenological components was able to simulate photosynthetic seasonality, explaining ~90% of the average seasonal variation in eddy covariance derived CO_2 assimilation. This work identifies a parsimonious approach for representing tropical evergreen forest photosynthetic seasonality in TBMs that utilize the FvCB model of CO_2 assimilation, and highlights the importance of incorporating more

49 realistic phenological mechanisms in models that seek to improve the projection of future carbon
50 dynamics in tropical evergreen forests.

51 **1. Introduction**

52 Tropical evergreen forests play a dominant role in the global carbon, water, and energy
53 cycles (Pan *et al.*, 2011; Fu *et al.*, 2013; Stark *et al.*, 2016). They account for around one-third of
54 annual terrestrial photosynthesis (Beer *et al.*, 2010) and a quarter of the global aboveground
55 carbon stock (Saatchi *et al.*, 2011; Aragao *et al.*, 2014). Therefore, even small errors in model
56 representation of the carbon pools or fluxes in this biome will result in marked uncertainty in the
57 projection of future climate (Friedlingstein *et al.*, 2006, 2014; Cox *et al.*, 2013; Huntingford *et*
58 *al.*, 2013). A key area of uncertainty is our understanding and model representation of tropical
59 evergreen forest seasonality, including seasonal leaf display as well as physiological function
60 (Saleska *et al.*, 2003; Restrepo-Coupe *et al.*, 2013; Guan *et al.*, 2015). Most Terrestrial Biosphere
61 Models (TBMs) have a mechanistic representation of CO_2 assimilation that is capable of
62 simulating the response of photosynthesis to global change (e.g. increasing atmospheric CO_2
63 concentration). However, most of these models lack mechanistic representation of tropical forest
64 photosynthetic seasonality (de Weirdt *et al.*, 2012, Kim *et al.*, 2012; Restrepo-Coupe *et al.*,
65 2017). To improve our ability to project the impact of global change on the terrestrial carbon
66 cycle, we need to integrate model representation of the mechanisms that regulate tropical forest
67 photosynthetic seasonality with an approach that is capable of mechanistically representing the
68 response of photosynthesis to global change.

69 Within tropical evergreen forests, leaf production from field based studies (e.g. Wright &
70 van Schaik, 1994; Girardin *et al.*, 2016), and canopy photosynthesis (i.e. gross primary
71 productivity, GPP) derived from eddy flux towers (Saleska *et al.*, 2003; Hutyra *et al.*, 2007;
72 Restrepo-Coupe *et al.*, 2013) and satellites (Lee *et al.*, 2013; Guan *et al.*, 2015) consistently
73 show seasonal variability. Importantly, this seasonal variation is not directly related to extrinsic

74 environmental variability (Bradley *et al.*, 2011; Guan *et al.*, 2015; Wu *et al.*, 2016a, 2017).
75 Instead, increasing evidence has shown that tropical leaf phenology is a primary mechanism
76 regulating seasonal carbon assimilation (Doughty & Goulden, 2008; Kim *et al.*, 2012; Restrepo-
77 Coupe *et al.*, 2013; Wu *et al.*, 2016a, 2017). Here phenology refers to periodic cycles of leaf
78 production, development and abscission within a forest canopy, which produces seasonal
79 variability in leaf quantity (i.e. canopy leaf area index, LAI) and leaf quality (i.e. per-area leaf
80 photosynthetic capacity), and includes the differential leaf turnover associated with the changes
81 in leaf longevity within vertical canopy profiles. Despite a modest seasonality in leaf quantity
82 (e.g. Doughty & Goulden, 2008; Brando *et al.*, 2010; Lopes *et al.*, 2016; Saleska *et al.*, 2016),
83 many tropical evergreen forests exhibit substantial leaf turnover during the dry season when
84 monthly precipitation is lower than the evaporative demand (Borchert, 1994; Wright & van
85 Schaik, 1994; Wu *et al.*, 2016a; Lopes *et al.*, 2016). As a result, these forests have a strong
86 seasonality in leaf quality because recently mature leaves have a higher photosynthetic capacity
87 than the old leaves they replace (Kitajima *et al.*, 1997a; Doughty & Goulden, 2008; Wu *et al.*,
88 2016a). Importantly, this seasonal variation in leaf quality was recently shown to be one of the
89 most important phenological mechanisms responsible for photosynthetic seasonality in tropical
90 evergreen forests (Wu *et al.*, 2016a, 2017). However, this advance (e.g. Wu *et al.*, 2016a, 2017)
91 was based on a light use efficiency model that can capture tropical forest photosynthetic
92 seasonality but lacks the physiological and structural complexity that is necessary to project the
93 response to the changing climate, particularly rising CO_2 concentration.

94 In addition to leaf quality and quantity, the within canopy variation in leaf longevity has
95 been well documented in the tropics (e.g. Lowman, 1992; Miyaji *et al.*, 1997; Reich *et al.*, 2004).
96 This large within-canopy variation in leaf phenological characteristics, with understory leaves

97 living two or more times longer than canopy leaves, may be attributed either to temporal niche
98 partitioning between canopy trees and the understory (Messier *et al.*, 1998; Augspurger *et al.*,
99 2005; Richardson & O'Keefe, 2009), or to an adaptive response to large within-canopy variation
100 in environmental variables (Wright *et al.*, 2006; Stark *et al.*, 2012, 2015; Niinemets *et al.*, 2015).
101 As such, within-canopy variation in light and associated biotic properties have also been
102 suggested as an important control on processes such as leaf development, energy balance, water
103 use, and photosynthesis (Ellsworth & Reich, 1993; Baldocchi & Amthor, 2001; Stark *et al.*,
104 2012; Morton *et al.*, 2016).

105 Despite the importance of leaf phenology in regulating photosynthetic seasonality in the
106 tropics, the combined effects of these three phenological components on tropical forest
107 photosynthetic seasonality are either absent or have not been adequately represented in current
108 TBMs (e.g. Restrepo-Coupe *et al.*, 2017). The majority of TBMs (e.g. Fisher *et al.*, 2015; Rogers
109 *et al.*, 2017) utilize the Farquhar, von Caemmerer and Berry (1980) (FvCB) leaf scale
110 mechanistic model of CO_2 assimilation to simulate carbon uptake together with a leaf to canopy
111 scaling relationship, which often represents the whole forest canopy as sunlit and shade leaf
112 fractions (e.g. dePury & Farquhar, 1997; Drewry *et al.*, 2010). Several modeling attempts have
113 been proposed to improve the representation of photosynthetic seasonality. For example, some
114 TBMs have included seasonal variation in LAI driven by water availability (Baker *et al.*, 2008;
115 Powell *et al.*, 2013; Sitch *et al.*, 2015; Xu *et al.,* 2016; Restrepo-Coupe *et al.*, 2017); however,
116 the representation of seasonal change in leaf quality and their vertical distribution has rarely been
117 explored before. As a result, these models generally fail to adequately reproduce the
118 photosynthetic seasonality of tropical evergreen forests, simulating a dry-season photosynthetic
119 decrease as a consequence of increasing dry-season water stress, with eddy covariance derived

120 GPP showing the opposite trend (Saleska *et al.*, 2003; Baker *et al.*, 2008; de Goncalves *et al.*,
121 2013; Restrepo-Coupe *et al.*, 2017). Several other attempts have shown some improvement in the
122 modeling performance of TBM-based photosynthetic seasonality by tuning model parameters to
123 allow for seasonal variation in leaf photosynthetic capacity (e.g. de Weirdt *et al.,* 2012; Kim *et*
124 *al.*, 2012). However, the assumptions made in these models, such as the application of the leaf
125 economic spectrum to within-canopy relationships, require systematic evaluation (Messier *et al.*,
126 2016) or compared to field based metrics of both leaf phenology (e.g. leaf production and
127 senescence) and GPP. The model-observation mismatch and the incomplete mechanistic
128 evaluation highlight need for improving current TBMs which should include a mechanistic
129 representation of leaf phenology effects on tropical evergreen forest photosynthesis that includes
130 all three phenological components of leaf quantity, quality, and differential leaf turnover within a
131 forest canopy.

132 The goal of this study was to develop an approach that would provide the sufficient
133 phenological representation of the three components to capture the photosynthetic seasonality of
134 a tropical evergreen forest in a mechanistic model framework that included the FvCB
135 representation of CO_2 assimilation and a multilayer canopy. We accomplished this by evaluating
136 the performance of model structures that incorporated the three different phenological
137 mechanisms. We asked three questions: (1) Is seasonality of tropical forest photosynthesis
138 reproduced by a model including leaf phenology? (2) What is the relative contribution of these
139 three phenological components in controlling the seasonality of photosynthesis? (3) Finally, how
140 do these three components regulate tropical forest photosynthetic seasonality?

141 Our approach was to modify existing canopy photosynthesis models to enable coupling
142 with prescribed, field-based phenology of the leaf quantity and quality allowing us to simulate

canopy photosynthetic seasonality. In addition, we enabled representation of sun and shade leaf fractions and a two-layer canopy (upper and lower) to allow us to explore within-canopy phenological variation. As such, our model framework allowed us to assess how the three components of leaf phenology independently and jointly regulated canopy-scale photosynthetic seasonality. In order to evaluate the model performance and avoid other confounding factors in our analysis, such as seasonal and inter-annual environmental variation (Baldocchi & Amthor, 2001; Richardson *et al.*, 2007; Wu *et al.*, 2017), our target variable was GPP_{ref}, which is eddy covariance derived or modeled GPP under a reference environment. This enabled us to focus on the underlying physiological mechanisms and isolate the biological controls on GPP from seasonality in environmental variables (Wu *et al.*, 2017). The successful attribution of biological controls on tropical forest photosynthesis will not only improve modeling of photosynthesis in the tropics but also help assess the correct functional response to environmental variability.

2. Materials and Methods

2.1 Model evaluation

To evaluate model performance we used data from the Tapajós k67 eddy covariance (EC) tower site (with Fluxnet2015 ID of "BR-Sa1"; http://fluxnet.fluxdata.org/data/download-data/). The k67 EC tower site (54°58'W, 2°51'S) is located in the Tapajós National Forest, near Santarém, Pará, Brazil. Tapajós is an evergreen tropical forest on a well-drained clay-soil plateau (Rice *et al.*, 2004), with a mean upper canopy height of ~40 m (Hutyra *et al.*, 2007). Mean annual precipitation is ~2000 mm $year^{-1}$ with a 5-month dry season (monthly precipitation < monthly evapotranspiration) from approximately mid-July to mid-December (Hutyra *et al.*, 2007; Restrepo-Coupe *et al.*, 2013).

166 The k67 EC site included seven-full-year flux and meteorological measurements (years
167 2002-2005, and 2009-2011; Wu *et al.*, 2016a, 2017). Detailed descriptions of the instrumentation
168 and data pre-processing protocol for the k67 EC data can be found in Hutyra *et al* (2007) and
169 Restrepo-Coupe *et al* (2013). No gap-filling data was used in this study. Hourly EC
170 measurements of net ecosystem exchange (NEE) was partitioned into ecosystem respiration
171 (R_{eco}) and GPP following standard approaches (Hutyra *et al.*, 2007; Restrepo-Coupe *et al.*,
172 2013): Reco, which was averaged within monthly bins from valid nighttime hourly NEE during
173 well-mixed periods (u* criterion: ≥0.22 m/s), was also used as an estimate of average monthly
174 daytime respiration, and GPP was estimated as -(NEE – Reco). We did not use a temperature
175 function to extrapolate nighttime NEE to daytime Reco, as is done at many higher latitude sites
176 (e.g. Reichstein *et al.,* 2005), because nighttime temperature range within most months at k67 is
177 too small to constrain such a function (Hutyra *et al.*, 2007). Also because Reco is composited by
178 the two components: (1) the heterotrophic component (which is expected to have higher values
179 in the daytime, due to higher temperature in the daytime than at night; Reichstein *et al.,* 2005),
180 and (2) the autotrophic component, especially the part associated with foliar respiration (which is
181 expected to have lower values in the daytime, due to light-inhibition of mitochondrial respiration
182 in leaves; Heskel *et al.*, 2013*;* Wehr *et al.*, 2016), therefore, without the specific information
183 about the relative contribution of these two components, we judged that our approach (using
184 unmodified nighttime values as estimates for daytime Reco) was conservative – especially for a
185 study of seasonality, for which potential errors in absolute value are less important.

186 In this study we used the reference GPP (GPP_{ref}) as our target variable and benchmark for
187 model evaluation. GPP_{ref} represents the CO_2 assimilation of the canopy in the absence of
188 environmental fluctuations and thus provides the capability to evaluate the phenological impact

on canopy-scale photosynthesis independent of other sources of variation. EC-derived GPP_{ref} was calculated as the monthly average of all seven-year EC-derived GPP measurements under a reference environmental condition, following Wu *et al* (2016a, 2017). The EC-derived GPP_{ref} here scales linearly with incident light-use-efficiency under the reference environment as used in Wu *et al* (2016a, 2017) (where it was called canopy-scale photosynthetic capacity). The reference environment for GPP_{ref} was taken as narrow bins of each climatic driver: canopy-top photosynthetically active radiation (PAR_0)=1320 ± 200 μmol $m^{-2}s^{-1}$, diffuse light fraction=0.4 ± 0.1, vapor pressure deficit (VPD)=0.87 ± 0.20 kPa, air-temperature (T_{air})=28 ± 1 ºC, and solar zenith angle (SZA)=30 ± 5º, and 8.1% of all hourly EC-derived GPP measurements were selected under the reference environment (~20 measurements per month per year; almost equally distributed across months). We used the seven-year mean annual cycle of monthly EC-derived GPP_{ref} as a benchmark for model validation. The same reference environment is also used for our model simulation of canopy-scale GPP_{ref} (see "Model Framework" below).

2.2 Prescribed phenology

Three components of leaf phenology were examined in this study, including the quantity, the quality, and within-canopy variation in leaf turnover rates, all of which are tightly linked with seasonal variability in leaf production, development and abscission within a tropical forest canopy (Wu *et al.*, 2016a,b; Lopes *et al.*, 2016). Our prescribed, field-based leaf phenology data at the k67 site are the same as those used in Wu *et al* (2016a).

(1) Field data of canopy LAI, litterfall LAI, and new leaf LAI. The mean annual cycle of monthly canopy LAI (range: 5.35–6.15 m^2 m^{-2}) was derived from tower-mounted camera image timeseries (Tetracam Agricultural Digital Camera, Tetracam, Inc., Gaomesville, FL; January

212 2010 to December 2011) using a camera-based tree inventory approach. For details about this
213 approach, please refer to supplementary materials section 5 and Figs. S5 and S8 in Wu *et al*
214 (2016a). The mean annual cycle of monthly litterfall LAI (range: 0.23–0.66 m^2 m^{-2}) was derived
215 by converting field observations of mass-based foliage litterfall (Mg biomass $month^{-1}$ ha^{-1}; bi-
216 weekly measurements from 2001 to 2005; Brando *et al.*, 2010) of the same site into area-based
217 litterfall LAI (m^2 m^{-2} per month), with the formula of Litterfall LAI = mass-based
218 Litterfall×SLA, applying a mean specific leaf area (SLA) of 0.816 ha Mg^{-1} biomass (Malhado *et*
219 *al.*, 2009). The mean annual cycle of monthly new leaf LAI production (in m^2 m^{-2} per month)
220 was estimated by using the formula of dLAI/dt + litterfall LAI, where dLAI/dt is the average
221 canopy LAI change in the two months centered around LAI of each month (Wu *et al.*, 2016a).
222 (2) Field based leaf gas exchange measurements. Leaf level photosynthetic capacity,
223 represented by the apparent maximum carboxylation capacity of Rubisco standardized to a
224 reference temperature of 25°C (V_{cmax25}) (Bernacchi *et al.*, 2013), was derived from standard leaf
225 gas exchange measurements of photosynthetic CO_2 response curves (A-C_i) for top-of-canopy
226 sunlit leaves of five canopy trees at the k67 site (species and structural information for leaf
227 samples are shown in Table S1; data are available from
228 http://datadryad.org/resource/doi:10.5061/dryad.8fb47; see supplementary materials in Wu *et al*,
229 2016a for more details on these data). Briefly, the trees we targeted for *A-Ci* curves represent the
230 most abundant species that account for ~24% of the local basal area (Pyle *et al.*, 2008). Prior to
231 gas exchange measurements, branches (of ~ 1m length) were assessed using arborist climbing
232 methods, cut, then promptly but gently lowered to the ground with ropes, and re-cut under water
233 at least once within 15 minutes of the initial harvest. Gas exchange was typically measured for
234 leaves of each age category present on the branch. These sunlit leaves (n=27) were initially

classified into three age classes (Young, Mature, and Old) based on visual assessment of color, size, rigidity, and bud scars (when present) (Chavana-Bryant *et al.*, 2016), and then confirmed by in-situ leaf tagging and associated photographic imaging of leaves at known ages (from 10 days old up to 1 year old; see Wu *et al.*, 2016b for more details). These leaf age classes roughly correspond to a young age class (leaves of 1-2 months old), a mature age class (leaves of 3-5 months), and an old age class (leaves of ≥6 months). Very young leaves (recent leaf burst; e.g. Fig. S1 in Wu *et al.*, 2016b) were too small, delicate, or logistically challenging for photosynthesis measurements, therefore field derived leaf V_{cmax25} of the young age class (which corresponds to the young leaves of late stage, big enough for Licor measurements) was then divided by two to provide an average across the distribution of the entire young age class. The five-species mean (± standard deviation) V_{cmax25} for these top-of-canopy sunlit leaves of young, mature, and old age classes were 6.8 (±1.4), 36.5 (±10.7), and 23.4 (±5.1) μmol CO_2 m^{-2} s^{-1}, respectively.

(3) The mean seasonality of leaf age demographics and leaf quality. The quality component of leaf phenology refers to per-area leaf photosynthetic capacity. At the canopy scale, leaf quality can be approximated by the age-dependency of leaf photosynthetic capacity (shown above) and the associated leaf age fraction (or leaf age-demography). Leaf age demographics were approximated by a three-LAI-age-class demography model (Wu *et al*, 2016a), with the inputs from mean annual cycles of monthly canopy LAI and new leaf LAI (calculated above). The model-derived three LAI-age demographics include the LAI for a young age class (leaves of 1-2 months old, LAI_Y), a mature age class (leaves of 3-5 months, LAI_M), and an old age class (leaves of ≥6 months, LAI_O; see Fig. 1), with the two optimized model parameters from Wu *et al* (2016a) which define leaf residence time at young and mature age classes respectively. The

258 reason we use these optimized parameters here is because these parameters were consistent with
259 our field observations of leaf aging processes (Chavana-Bryant *et al.*, 2016; Wu *et al.*, 2016b), as
260 well as the roughly similar time interval of mature and old leaf age classes for field-based leaf
261 gas exchange measurements.

262 In sum, the leaf quality was calculated by using a three-age-class leaf demography-
263 ontogeny model as below (Wu *et al*, 2016a).

264 $$Lquality = \frac{V_{cmax,Y} \times LAI_Y + V_{cmax,M} \times LAI_M + V_{cmax,O} \times LAI_O}{LAI_Y + LAI_M + LAI_O} \quad (1)$$

265 Where *Lquality* is leaf quality, which represents age composition weighted leaf photosynthetic
266 capacity, and $V_{cmax,Y}$, $V_{cmax,M}$, and $V_{cmax,O}$ represent leaf level V_{cmax} at young, mature and old age
267 classes respectively.

268

269 2.3 Model framework

270 2.3.1 TBM-type canopy photosynthesis models (DF1997 and ML)

271 Sun-shade, big leaf, canopy photosynthesis models, which represent the whole forest
272 canopy as a big leaf of the two fractions (sun versus shade), are commonly used in many TBMs,
273 e.g. Community Land Model version 4.5 (CLM4.5; Oleson *et al.*, 2013) and the Joint UK Land
274 Environmental Simulator version 4.5 (JULES4.5; Best *et al.*, 2011; Clark *et al.*, 2011; Harper *et*
275 *al.*, 2016). Canopy photosynthesis is usually represented in these formulations by the two
276 processes: a leaf scale mechanistic photosynthesis model and a leaf-canopy scaling relationship,
277 which represents the whole forest canopy as sunlit and shade fractions using approaches such as
278 dePury and Farquhar (1997; DF1997) or a multi-layer approach (Drewry *et al.*, 2010; ML).
279 These processes are described in detail as below.

280 (1) A leaf scale mechanistic photosynthesis model. Here we couple a mechanistic FvCB
281 based photosynthesis model with a stomatal conductance scheme (Medlyn *et al.*, 2011; Lin *et al.*,
282 2015) to simulate the leaf level photosynthesis response to the variability in both biotic (e.g.
283 V_{cmax25} and J_{max25}) and climatic (e.g. PAR, temperature and VPD) factors (details in Table S2).
284 The Medlyn-type stomatal conductance model was selected because leaves/stomata respond to
285 VPD rather than relative humidity. Therefore, the Medlyn-type stomatal conductance model will
286 likely capture projected increases in VPD better than other alternatives (Rogers *et al.*, 2017). The
287 only prescribed parameter of this stomatal conductance model is the stomatal slope, and here we
288 used the value of 3.77 based on a recent meta-data analysis for tropical rainforest trees (Lin *et*
289 *al.*, 2015). Additionally, we refer to Lloyd & Farquhar (2008) and Bernacchi *et al* (2013) to
290 describe the temperature effect on leaf photosynthesis. As such, this photosynthesis model has
291 the capability to simulate the leaf level photosynthetic response to the current environmental
292 variability, but also to the changing environmental drivers associated with global change (i.e.
293 rising CO_2 concentration, temperature and VPD).

294 (2) The leaf to canopy scaling relationship represented by the DF1997 model. DF1997
295 simulates canopy photosynthesis as the sum of the photosynthetic rate contributed by the sunlit
296 fraction (GPP_{sun}) and the shade fraction (GPP_{shade}) of a forest canopy respectively (eqn. 2).

297 $$GPP = GPP_{sun} + GPP_{shade} \quad (2)$$

298 The DF1997 model is operated by firstly determining the LAI, V_{cmax} and absorbed PAR
299 for each canopy fraction, and then applying leaf level photosynthesis model (as above) to
300 simulate the photosynthesis to each canopy fraction. Canopy total LAI (LAI_{tot}) is partitioned into
301 the sunlit fraction (LAI_{sun}) and the shade fraction (LAI_{shade}), following Beer's law (eqns. 3-4;
302 dePury & Farquhar, 1997; Chen *et al.*, 1999; Ryu *et al.*, 2011):

$$LAI_{sun} = \frac{1 - \exp(-\frac{k \times \Omega \times LAI_{tot}}{\cos(SZA)})}{k / \cos(SZA)} \quad (3)$$

$$LAI_{shade} = LAI_{tot} - LAI_{sun} \quad (4)$$

where k(=0.5) is the extinction coefficient, and Ω is the clumping index; Ω=0.66 for tropical evergreen forest (He *et al.*, 2012) was used in this study.

DF1997 also partitions the canopy integrated V_{cmax} ($V_{\mathrm{cmax,tot}}$) into the sunlit fraction ($V_{\mathrm{cmax,sun}}$) and the shade fraction ($V_{\mathrm{cmax,shade}}$) (see Table S3). Here we assumed that V_{cmax} declines exponentially within the canopy following Lloyd *et al* (2010) (see eqns. 5-6 below; Fig. 2).

$$V_{c\max,i} = V_{c\max,0} \times \exp(-k_n \times LAI_i) \quad (5)$$

$$k_n = \exp(0.00963 \times V_{c\max,0} - 2.43) \quad (6)$$

where $V_{c\max,0}$ is the V_{cmax} of leaves at the top of the canopy; and k_n describes the exponential decline of V_{cmax} against the given accumulated LAI from the top of the canopy (LAI_i). By tracking PAR at the top of the canopy (PAR_0), which is the sum of direct beam ($PAR_{b,0}$) and diffuse radiation ($PAR_{d,0}$) in the visible spectrum (i.e. 400-700 nm), DF1997 calculates its canopy absorbance by the sunlit fraction (PAR_{sun}) and by the shade fraction (PAR_{shade}), using Beer's law and Seller's (1987) two-stream approximation for canopy radiative transfer (dePury & Farquhar, 1997; Ryu *et al.*, 2011; Tables S4-S5).

To facilitate the simulation of photosynthetic seasonality with DF1997, we prescribed top-of-canopy $V_{\mathrm{cmax,0}}$ (in eqn. 5), i.e. *Lquality* (eqn. 1), while assuming that vertical changes in V_{cmax} within a forest canopy follow a fixed exponential decline rate (as described by eqns. 5-6). The complete equation set for the DF1997 model is provided in Tables S2-S5.

(3) The leaf-canopy scaling relationship represented by the multi-layer model. ML is an alternative way to scale leaf-level function and simulate canopy photosynthesis. ML explicitly

resolves direct and diffuse radiation for sunlit and shade canopy fractions at each canopy layer using Seller's (1987) two-stream approximation for canopy radiative transfer. The number of canopy layers is prescribed as N, where initial results from a model sensitivity showed that GPP was insensitive to N $\geq$ 15 (Fig. S1). We thus used N=15 for the following simulations. In addition, we calculated the LAI of the sunlit ($LAI_{sun,i}$) and the shaded ($LAI_{shade,i}$) fractions for each canopy layer *i* (i=1, 2,…, N), and their corresponding per-area radiation absorbed by the sunlit fraction ($PAR_{sun,i}$) and the shade fraction ($PAR_{shade,i}$). Last, ML calculated the V_{cmax} of each canopy layer ($V_{cmax,i}$) also using eqns. 5-6.

The leaf level photosynthesis model was then used to calculate the photosynthesis rate of each canopy fraction for given layer *i*: per-area photosynthesis rate for the sunlit ($GPP_{sun,area,i}$) and the shade ($GPP_{shade,area,i}$). The cumulative canopy photosynthesis rate was thus equal to the sum of area weighted photosynthesis rate of each layer:

$$GPP = \sum_{i=1}^{N} (GPP_{sun,area,i} \times LAI_{sun,i} + GPP_{shade,area,i} \times LAI_{shade,i}) \tag{7}$$

To facilitate the simulation of photosynthetic seasonality with ML, we also prescribed top-of-canopy $V_{\mathrm{cmax},0}$ (in eqn. 5), i.e. *Lquality* (eqn. 1).

It is important to note that the models (DF1997 and ML) presented here can simulate leaf phenology effects of both quantity and quality components; however, none of these models accounted for within-canopy phenological variation, and assumed a constant leaf turnover (flushing and abscission) rate throughout the canopy. Additionally, in our model simulation, we assume that leaf temperature and VPD for the sunlit and shade canopy fractions are the same as the reference environment.

347 2.3.2 Modified TBM representation of canopy photosynthesis to allow for within-canopy
348 phenological variation (a two-fraction leaf, two-layer canopy model)

349 Many field-based studies have indicated that leaf longevity could vary greatly depending
350 on the growth environments (e.g. Wright *et al.*, 2006; Wu *et al.*, 2016b), with understory leaves
351 displaying longer leaf longevity than upper canopy leaves (Lowman, 1992; Miyaji *et al.*, 1997;
352 Reich *et al.*, 2004). This suggests that the leaf turnover rate in the upper canopy should be faster
353 than that in the lower canopy and understory. However, the within-canopy phenological variation
354 has not been explicitly accounted for until now. To accomplish this, we modified the ML model
355 framework (via addition of a second, lower canopy layer) to allow explicit representation of
356 within-canopy variation in leaf turnover, in addition to the sun andshade fractions that already
357 allow for within-canopy physiological variation.

358 In this new model, we divided a forest canopy into the two layers: (1) the upper canopy
359 layer with the cumulative LAI from 0 (top-of-canopy) to 2.5 m^2 m^{-2}, and (2) the lower canopy
360 layer including the remainder of the canopy. Both layers are assumed to have the same
361 phenological pattern and timing, but the amount of leaf flush and litterfall that drives phenology
362 is differentially allocated between them. This allocation between layers is specified by ftop, the
363 fraction of observed leaf turnover (including leaf drop and flush) across the whole forest canopy
364 attributed to leaves in the upper canopy layer, e.g. when ftop = 0.7, 70% of observed forest
365 canopy leaf turnover (and associated amplitude of the LAI and *Lquality* variables) is attributed to
366 the upper canopy layer and 30% to the lower canopy layer; under this case, the ratio of leaf
367 turnover rate between upper canopy leaves and lower canopy leaves can be calculated as
368 (ftop/LAI_up)/((1-ftop)/LAI_low)=2.8, where ftop=0.7, LAI_up (or the average LAI for the
369 upper canopy layer)=2.5 m^2 m^{-2}, and LAI_low (or the average LAI for lower canopy layer)=3 m^2

370 m^{-2}. Since leaf longevity is an inverse of leaf turnover rate, therefore the leaf longevity for the
371 lower canopy leaves is around 2.8 times longer than the upper canopy leaves when ftop=0.7. Our
372 differentiation of these two canopy layers (upper and lower) at the LAI cutoff of 2.5 m^2 m^{-2} for
373 the upper canopy is slightly arbitrary, but sensitivity analysis showed that our modeling results
374 were largely insensitive to the LAI cutoff and exhibited only minor variation when LAI
375 increased from 2 to 3 m^2 m^{-2} (Fig. S2).
376
377 2.4 Model experiments
378 We used our proposed two-fraction leaf, two-layer canopy model as the main modeling
379 testbed for assessing the effect of different phenological components on modeled canopy
380 photosynthetic seasonality. This is because previous studies (e.g. dePury and Farquhar, 1997;
381 Bonan *et al.*, 2012) demonstrate that DF1997 and ML can simulate almost identical GPP fluxes
382 at the canopy scale (which is also confirmed by our Fig. S3), and also because our proposed two-
383 fraction leaf, two-layer canopy model here is identical to ML when no within-canopy
384 phenological variation is considered but also enables to examine the effect of within-canopy
385 phenological variation by varying ftop. First, we ran the model parameterized by all three
386 components, aiming to explore how well the model with all phenological mechanisms can
387 capture EC-derived GPP_{ref} seasonality. The model inputs for these phenological components
388 include: (1) the leaf quantity based on field measurements of the mean annual cycle of monthly
389 LAI, (2) the leaf quality based on field-derived seasonality of *Lquality* (as calculated by eqn. 1,
390 weighted by field-measured age dependency of V_{cmax25} and field-derived leaf age demographics),
391 and (3) the within-canopy phenological variation, by assuming leaves of lower canopy layer had
392 2.8 times longer leaf longevity compared with that of upper canopy layer (or ftop=0.7), which is

393 consistent with the literature (e.g. Lowman, 1992; Miyaji *et al.*, 1997; Reich *et al.*, 2004). We
394 also ran the models under two additional scenarios, aiming to explore the relative role of each
395 phenological component on modeled photosynthetic seasonality, with that (1) the model is
396 parameterized with the observed annual cycle of leaf quantity alone, while assuming neither
397 within-canopy variation in leaf longevity nor seasonal variation in leaf quality, and that (2) the
398 model is parameterized with the observed phenological cycles of leaf quantity and quality, while
399 assuming a constant leaf turnover rate throughout the canopy. To further elucidate the
400 mechanisms by which each phenological component regulates canopy photosynthetic
401 seasonality, we also evaluated the GPP_{ref} sensitivity of the sunlit canopy fraction and the shade
402 canopy fraction to the seasonal variation in leaf phenology (quantity and quality) and within-
403 canopy variation in leaf longevity (by varying ftop from 0 to 1.0 with the increment of 0.1)
404 respectively.
405

406 **3. Results**

407 3.1 Modeled GPP_{ref} seasonality parameterized by differential leaf phenological mechanisms

408 We used the two-fraction leaf, two-layer canopy model to explore how including model
409 representation of the three different phenological components affected the ability of the models
410 to simulate the canopy scale photosynthetic seasonality, as compared with EC-derived GPP_{ref}.
411 Our results show that the model parameterized by all three phenological components (i.e.
412 quantity, quality and within-canopy phenological variation) was best able to capture EC-derived
413 photosynthetic seasonality (Fig. 3 and Table 1).

414 The seven-year mean annual cycle of EC-derived GPP_{ref} at the Tapajós k67 site showed
415 an initial decline in the late wet season, and then an increase in the dry season (Fig. 3). The

models parameterized by leaf quantity alone or parameterized by both leaf quantity and quality displayed good agreement with the timing of EC-derived GPP_{ref} seasonality, but missed the depth or relative magnitude of GPP_{ref} seasonality: leaf quantity phenology alone explained only 19% of EC-derived GPP_{ref} seasonality for DF1997 (Table 1) and 17% for ML and the two-fraction leaf, two-layer canopy model (Table 1 and Fig. 3a); the modeled GPP_{ref} with both leaf quantity and quality (but no within-canopy phenological variation) explained ~80% of EC-derived GPP_{ref} seasonality for DF1997, ML, and the two-fraction leaf, two-layer canopy model (Table 1 and Fig. 3b). The modeled GPP_{ref} using the two-fraction leaf, two-layer canopy model with all three phenological components displayed the strongest agreement with the seasonal variability of EC-derived GPP_{ref} in both timing and relative magnitude (R^2=0.90; Table 1 and Fig. 3c).

3.2 Differential photosynthetic sensitivity to seasonal variation in leaf phenology between the sunlit canopy fraction and the shade canopy fraction

To better understand the mechanisms that underlie canopy-scale photosynthetic seasonality, we examined the photosynthetic sensitivity of the sunlit canopy fraction and the shade canopy fraction to seasonal variation in leaf phenology (quantity and quality). We theorized that the seasonal variation in GPP_{ref} is driven by changes in both canopy absorbed PAR (affecting RuBP regeneration limited photosynthesis in the FvCB model) and canopy integrated V_{cmax} (affecting Rubisco limited photosynthesis in the FvCB model). Fig. 4 summarizes our model diagnosis of these two pathways and their respective influence on modeled GPP_{ref} seasonality.

438 First we examined the seasonal dynamics of canopy absorbed PAR under reference
439 environmental conditions (absolute value in Fig. 4a and relative value in Fig. S4). Our
440 simulations showed that the PAR absorbed by the sunlit canopy fraction (PAR_{sun}), the shade
441 canopy fraction (PAR_{shade}), and the entire canopy (PAR_{sun} +PAR_{shade}) all showed consistently low
442 seasonal variability (<6%; Fig. 4a and Fig. S4), despite modest seasonal variability in leaf
443 quantity (~12%; Fig. 4b). This is likely because tropical evergreen forests display consistently
444 high leaf quantity over the annual cycle (e.g. LAI range: 5.35-6.15 m^2 m^{-2} at the k67 site), and as
445 such annual FAPAR is typically at or near saturation.

446 We then investigated the seasonal dynamics of canopy V_{cmax}, which is the integrated sum
447 of leaf level V_{cmax} weighted by the total LAI attributed to the sunlit fraction and the shade
448 fraction respectively (see eqns 3-5). Focusing first on the sunlit fraction, Fig. 4b highlights that
449 the LAI_{sun} is generally stable (~1.5 m^2 m^{-2}) through the annual cycle, despite the observed modest
450 seasonality in total canopy leaf quantity (LAI_{tot} = LAI_{sun}+ LAI_{shade}). As a consequence, the
451 observed higher seasonal variability (~20%) in $V_{\mathrm{cmax,\ sun}}$ (Fig. 4c) is primarily driven by leaf
452 quality, which is associated with seasonal variation in leaf age demographics (Fig. 1 and eqn. 1).
453 In addition, our results indicated that the higher seasonal variability (~25%) in $V_{\mathrm{cmax,\ shade}}$ (Fig.
454 4c) is a consequence of seasonal variability in both LAI_{shade} (Fig. 4b) and leaf age demographics
455 (Fig. 1 and eqn. 1).

456 Finally, we assessed the seasonal variability in GPP_{ref} as the joint response to the above
457 two dynamics: canopy absorbed PAR and V_{cmax}. We used the FvCB model to calculate the GPP_{ref}
458 of both fractions (sun vs. shade). Sensitivity analysis of the FvCB model (Fig. S5) showed that
459 the canopy integrated absorbed PAR and canopy integrated V_{cmax} jointly regulated GPP_{ref}, with
460 canopy integrated V_{cmax} dominating the GPP_{ref} response under high light condition (i.e.

461 PAR>800 μmol m^{-2} s^{-1}) while canopy integrated absorbed PAR dominated GPP_{ref} response under
462 low light condition (i.e. PAR<400 μmol $m^{-2}s^{-1}$). Given that the sunlit fraction could consistently
463 capture sufficient PAR to photosaturate photosynthesis (~860 μmol m^{-2} s^{-1}; Fig. 4a) over the
464 annual cycle, the seasonal variability in $GPP_{ref,\ sun}$ closely tracked the seasonality of $V_{cmax,sun}$
465 (Figs. 4c,d), which is mostly determined by the phenology of leaf quality (Figs. 4b,c). On the
466 other hand, since the shade fraction typically receives sub-saturating light (~300 μmol $m^{-2}s^{-1}$;
467 Fig. 4a) over the annual cycle, $GPP_{ref,\ shade}$ is primarily limited by the capacity for RuBP
468 regeneration (Fig. S5). As a result, modeled $GPP_{ref,\ shade}$ seasonality is small (~7%; Fig. S6),
469 which is comparable with the relative seasonal change in PAR_{shade} (~6%; Fig. S4), but far less
470 than the relative seasonality in $V_{cmax,\ shade}$ (25%; Fig. 4c). The canopy total GPP_{ref} thus showed an
471 intermediate seasonal variation, with the relative magnitude of annual change falling in between
472 that of the two fractions (absolute value in Fig. 4d and relative value in Fig. S6).
473
474 3.3 Model sensitivity of canopy photosynthesis to within-canopy phenological variations
475 Finally, we used the two-fraction leaf, two-layer canopy model to explore the extent to
476 which within-canopy phenological variations could affect modeled photosynthetic seasonality.
477 We show that although the timing of the modeled GPP_{ref} seasonality follows observed LAI and
478 LAI-age-demography (Fig. 1) and was independent of within-canopy phenological variation (i.e.
479 ftop), the relative magnitude of the modeled GPP_{ref} seasonality is highly sensitive to ftop (Fig.
480 5a). As ftop increases (more leaf turnover is partitioned to the upper canopy), the relative
481 magnitude of modeled GPP_{ref} seasonality increases (Fig. 5a). Meanwhile, the correlation
482 between modeled and EC-derived GPP_{ref} seasonality also increases with ftop and reaches near
483 saturation when ftop ≥0.7 (R^2=0.90; Fig. 5b). The underlying reason is associated with the

484 differential photosynthetic sensitivity to leaf quality allocated to the two canopy layers (upper vs.
485 lower): as shown in Fig. 4, only the photosynthetic rate of the sunlit fraction (mostly occupied in
486 the upper canopy layer) is predominantly Rubisco limited and therefore, the photosynthetic rate
487 of the upper canopy layer shows high sensitivity to leaf quality.
488

489 **4. Discussion**

490 Accurate model representation of the effects of leaf phenology on ecosystem
491 photosynthesis is a critical need for TBMs in general (Richardson *et al.*, 2012) and is essential,
492 necessary first step for capturing the timing and magnitude of seasonal variation in tropical forest
493 carbon fluxes (Restrepo-Coupe *et al.*, 2013, 2017; Fu *et al.*, 2013; Christoffersen *et al.*, 2014;
494 Wu *et al.*, 2016a). Here we developed a parsimonious approach to effectively couple the effects
495 of leaf phenology (i.e. quantity, quality and within-canopy variation) to the FvCB model for
496 simulating canopy-level photosynthetic seasonality. Our approach could be parameterized and
497 adopted within TBMs where it would enable improved representation and projection of the
498 response of tropical evergreen forest photosynthesis to global change.

499 Our results demonstrated that the proposed model (two-fraction leaf, two-layer canopy)
500 could effectively simulate EC-derived photosynthetic seasonality, only if the quality component
501 of leaf phenology was incorporated (Fig. 3 and Table 1). This is also consistent with previous
502 field-based remote sensing studies (Doughty & Goulden, 2008; Brando *et al.*, 2010; Lopes *et al.*,
503 2016; Saleska *et al.*, 2016), which highlight that variation in photosynthetic efficiency and the
504 spectral reflectance properties of leaves (Roberts *et al.*, 1998; Chavana-Bryant *et al.*, 2016; Wu
505 *et al.*, 2016a,b) may significantly contribute to explaining the satellite-detected dry season
506 "green-up" in tropical evergreen forests. In addition, our finding supports previous work which

507 showed that model representation of photosynthetic seasonality could be improved by tuning
508 model parameters to allow for seasonal variation in photosynthetic capacity, i.e. leaf quality
509 (Kim *et al.*, 2012; de Weirt *et al.*, 2012).

510 Although the models with different leaf phenological components were all able to
511 simulate the seasonal photosynthetic trend, the relative magnitude of modeled GPP_{ref} seasonality
512 varied strongly across the models (Fig. 3). The approach of incorporating all phenological
513 components (i.e. quantity, quality, and within-canopy variation) displayed the strongest
514 agreement with local EC-derived GPP_{ref}, while the approaches incorporating only part of the
515 three phenological components (e.g. leaf quantity alone in Fig. 3a and leaf quantity and quality
516 alone in Fig. 3b) only explained around half or less of the observed relative annual change
517 magnitude. These differences in model performance can be attributed to differential
518 photosynthetic sensitivity of the sunlit canopy fraction and the shade canopy fraction to seasonal
519 variation in leaf quantity, quality and within-canopy phenological variation, explained as below:

520 Leaf quantity. Our results show that there is only a weak effect of the quantity component
521 of leaf phenology on GPP_{ref} (Table 1). This is because tropical evergreen forests consistently
522 have high leaf quantity throughout the annual cycle (Myneni *et al.*, 1997; Doughty & Goulden,
523 2008; Brando *et al.*, 2010; Morton *et al.*, 2014; Bi *et al.*, 2015; Lopes *et al.*, 2016; Wu *et al.*,
524 2016a), and therefore the observed small seasonal changes in leaf quantity had little impact on
525 FAPAR seasonality (Fig. 4a and Fig. S4), and thus had little impact on GPP_{ref} seasonality.

526 Leaf quality. Our results show that the phenology of leaf quality is one of the dominant
527 drivers of canopy photosynthetic seasonality in tropical evergreen forests (Table 1), confirming
528 recent work (Wu *et al.*, 2016a). Using an FvCB-type canopy photosynthesis model (i.e. two-
529 fraction leaf, two-layer canopy model), we demonstrate that both light absorption and canopy

integrated V_{cmax} regulate canopy-scale photosynthesis rate (Fig. S5). However, only the upper, sunlit canopy fraction with sufficient light availability and absorption are limited by Rubsico (i.e. are light saturated) and show sensitivity to seasonal variation in leaf quality (i.e. V_{cmax}; Figs. 4, S5 and S6). In contrast, the shaded canopy fraction is predominantly limited by light and not by photosynthetic capacity, and consequently, increasing photosynthetic capacity in the shaded canopy fraction has little to no impact on the modeled GPP_{ref}. In other words, our results confirm the differential photosynthetic sensitivity to leaf quality between the sunlit and shade canopy fractions. Our finding is thus not consistent with the assumption made by Doughty & Goulden (2008), who assumed constant photosynthetic rates of the sunlit and shade canopy fractions with a single scalar to account for seasonal variation in leaf quality, and may explain why the approach of Doughty & Goulden (2008) overestimates the leaf quality effect for the shade canopy fraction.

Within-canopy phenological variation. Differential photosynthetic sensitivity of the sunlit and shade canopy fractions to leaf quality (as shown in Fig. 4) suggests that the return on investment for a new leaf is far greater if that leaf is flushed in the upper, sunlit canopy than in the shade, which was subsequently confirmed by our model sensitivity analysis of ftop (Fig. 5). This model sensitivity analysis demonstrated that by allowing for differential leaf turnover rates within the canopy, especially when attributing the majority of leaf turnover to the upper canopy, our model (two-fraction leaf, two-layer canopy) could markedly improve the model representation of photosynthetic seasonality (Figs. 3, 5). Importantly, our prescribed higher leaf turnover rate in the upper canopy (i.e. ftop=0.7) is also consistent with field-based studies in the tropics which show that the longevity of upper canopy leaves is markedly shorter than that of lower canopy leaves (Lowman, 1992; Miyaji *et al.*, 1997; Reich *et al.*, 2004).

553 Our analysis of the two-fraction leaf, two-layer canopy model further show that when the
554 majority of leaf turnover is allocated to the upper canopy, the whole forest tends to become more
555 Rubisco-limited and thus approaches a simpler one-layer big-leaf assumption, such as the model
556 presented in Wu *et al* (2016a). This explains why the simple model of Wu *et al* (2016a), which
557 does not contain explicit representation of within-canopy physiological and phenological
558 variation, still captured the seasonal cycle of GPP_{ref} in tropical evergreen forests. The approach
559 of Wu *et al* (2016a), which is based on empirical relationships, is a valuable approach for broad-
560 scale remotely sensed monitoring of tropical forest carbon cycling but lacks the capacity to
561 project tropical forest responses under future climates and global change. Thus a light-use
562 efficiency approach (e.g. Wu *et al.*, 2016a) is not as valuable for use within TBMs that typically
563 utilize the FvCB formulation of photosynthesis to simulate leaf and canopy photosynthesis
564 (Rogers *et al.*, 2017). Since TBMs need to project the response of photosynthesis to rising CO_2,
565 temperature, VPD and drought, they require more sophisticated approaches where key model
566 inputs, such as V_{cmax}, may be derived from trait databases, remote sensing, or internally
567 generated (i.e. prognostic) allowing coupling to biogeochemical processes (e.g. Fisher *et al.*,
568 2015; Serbin *et al.*, 2015; Ali *et al.*, 2016). Therefore, to accurately represent canopy
569 photosynthetic processes in tropical forests under a changing climate we advocate the use of the
570 approach outlined here, i.e. the two-fraction leaf, two-layer canopy model coupled to an FvCB
571 formulation with model representation of the three components of leaf phenology we identify
572 here.

573 Our work also highlights three important directions for future advances in model
574 representation of tropical evergreen forest photosynthesis. First, to minimize additional sources
575 of uncertainty when exploring approaches for the modeling of tropical forest photosynthetic

576 seasonality we utilized observed leaf phenology (e.g. Fig. 1). However, the ultimate mechanisms
577 that regulate seasonal variation in both tropical leaf quantity and quality are still largely
578 unknown. An improved and prognostic understanding and model representation of the
579 mechanisms that drive seasonal and inter-annual changes in leaf quantity and quality, i.e. the
580 drivers of broader-scale (i.e. regional and global) tropical evergreen forest phenology, will be a
581 key component in new models that seek to improve projections of carbon dynamics and potential
582 climate feedbacks in the tropics (Wu *et al.*, 2016a).

583 Second, our demonstration of the importance of leaf phenology effects on tropical forest
584 photosynthetic seasonality relied on modeled and EC-derived GPP_{ref}. This simplification was
585 essential to enable us to elucidate fundamental mechanisms connecting annual patterns of leaf
586 phenology with physiology, but is not appropriate when simulating forest responses to climate
587 over time or in response to climatic perturbations. Since canopy photosynthesis is jointly
588 determined by extrinsic environmental variability and changes in intrinsic photosynthetic
589 machinery (Farquhar *et al.*, 1980; Collatz *et al.*, 1991; Sellers *et al.*, 1992; dePury & Farquhar,
590 1997; Baldocchi & Amthor, 2001; Dai *et al.*, 2003; Medvigy *et al.*, 2009; Wu *et al.*, 2016a;
591 Rogers *et al.*, 2017), there is a great need to improve our understanding and model representation
592 of the fundamental physiological responses to environmental variability, particularly rising
593 atmospheric CO_2 concentration, temperature, VPD and changes in precipitation, but also light
594 capture and utilization by the forest canopy (Rogers *et al.*, 2017). It will be critical to link
595 advances in understanding of leaf phenology and physiology in future TBMs, particularly in
596 tropical evergreen forests.

597 Finally, our study also highlights that one of the most practical challenges limiting studies
598 in the tropics is the limited availability of observations (Schimel *et al.*, 2015). For example, there

599 is very little information available on the within-canopy (i.e. light-dependent vs. height-
600 dependent) and seasonal (i.e. continuous, age-dependency) variation in leaf physiology,
601 phenology, biochemical traits, and optical properties in the tropics (e.g. Kitajima *et al.*, 1997b;
602 Chavana-Bryant *et al.*, 2016; Wu *et al.*, 2016b); even less is known about the spatial
603 heterogeneity in the relationship among photosynthetic capacity, leaf traits, canopy structure,
604 phenology, and climate across broader-scale (i.e. regional and global) tropical forests (e.g.
605 Kumagai *et al.*, 2006; Kenzo *et al.*, 2015; Wu *et al.*, 2016b). As a consequence, some important
606 physiological mechanisms might be underrepresented in current models. For example, the study
607 presented by Kitajima *et al* (1997b) showed that leaf level Vcmax (at mature age class) for the
608 same tropical tree species can vary depends on the timing (i.e. wet or dry season) when leaves
609 are produced. This approach, also known as seasonal leaf phenotypes, suggested that leaf level
610 photosynthetic capacity should be modeled as a function of the timing when leaves are produced,
611 in addition to leaf age which has been explored in this paper. Our model framework has
612 sufficient flexibility to incorporate this additional component of photosynthetic seasonality, but
613 would require extensive field data and subsequent model evaluation to validate our approach.
614

615 **Acknowledgements:**

616 This work was supported by the Next-Generation Ecosystem Experiments–Tropics project
617 supported by the U.S. DOE, Office of Science, Office of Biological and Environmental Research
618 and through contract #DE-SC0012704 to Brookhaven National Laboratory. We also thank Drs.
619 Youngryel Ryu and Chongya Jiang for sharing their code of the dePury & Farquhar (1997)
620 model, which formed the initial base for our further coding development in this study. We also

thank three anonymous reviewers for their constructive comments to improve the scientific rigor and clarity of the manuscript.

Author Contributions:

J.W., A.R., S.P.S., and X.X. designed the research. J.W. and S.P.S. developed the Matlab and R codes of canopy photosynthesis model. J.W. performed the data analysis. J.W. drafted the manuscript, and A.R., S.P.S., S.R.S, X.X., L.P.A., M.C., and M.R. contributed to writing the final version.

References

Ali AA, Xu C, Rogers A, *et al.* (2016) A global scale mechanistic model of photosynthetic capacity (LUNA V1. 0). *Geoscientific Model Development*, **9**, 587-606.

Aragão LEOC, Poulter B, Barlow JB, *et al.* (2014) Environmental change and the carbon balance of Amazonian forests. *Biological Reviews*, **89**, 913-931.

Augspurger CK, Cheeseman JM, Salk CF (2005) Light gains and physiological capacity of understorey woody plants during phenological avoidance of canopy shade. *Functional Ecology*, **19**, 537-546.

Baldocchi DD, Amthor JS (2001) Canopy Photosynthesis: History. In: Terrestrial global productivity (eds Roy J, Saugier B, Mooney HA), pp.9-31. Academic Press, Waltham, MA

Baker IT, Prihodko L, Denning AS, *et al.* (2008) Seasonal drought stress in the Amazon: Reconciling models and observations. *Journal of Geophysical Research: Biogeosciences*, **113**, G00B01, doi: 10.1029/2007JG000644

Bernacchi CJ, Bagley JE, Serbin SP, *et al.* (2013) Modelling C3 photosynthesis from the chloroplast to the ecosystem. *Plant, cell & environment*, **36**, 1641-1657.

Best MJ, Pryor M, Clark DB, *et al.* (2011) The Joint UK Land Environment Simulator (JULES), model description–Part 1: energy and water fluxes. *Geoscientific Model Development*, **4**, 677-699.

Bi J, Knvazikhin Y, Choi S, *et al.* (2015) Sunlight mediated seasonality in canopy structure and photosynthetic activity of Amazonian rainforests. *Environmental Research Letters*, **10**, 064014, doi:10.1088/1748-9326/10/6/064014.

Bonan GB, Oleson KW, Fisher RA, Lasslop G, Reichstein M. (2012) Reconciling leaf physiological traits and canopy flux data: Use of the TRY and FLUXNET databases in the Community Land Model version 4. *Journal of Geophysical Research: Biogeosciences*, 117, G02026, doi:10.1029/2011JG001913.

Bradley AV, Gerard FF, Barbier N, *et al*, (2011). Relationships between phenology, radiation and precipitation in the Amazon region. *Global Change Biology*, **17**, 2245-2260.

Brando PM, Goetz SJ, Baccini A, *et al*. (2010) Seasonal and interannual variability of climate and vegetation indices across the Amazon. *Proceedings of the National Academy of Sciences of the United States of America*, **107**, 14685–14690.

Chavana-Bryant C, Malhi Y, Wu J, *et al*. (2016) Leaf aging of Amazonian canopy trees as revealed by spectral and physiochemical measurements. *New Phytologist*, doi:10.1111/nph.13853

Chen JM, Liu J, Cihlar J, Goulden ML (1999) Daily canopy photosynthesis model through temporal and spatial scaling for remote sensing applications. *Ecological modelling*, **124**, 99-119.

Christoffersen BO, Restrepo-Coupe N, Arain MA, *et al*. (2014) Mechanisms of water supply and vegetation demand govern the seasonality and magnitude of evapotranspiration in Amazonia and Cerrado. *Agricultural and Forest meteorology*, **191**, 33-50.

Clark DB, Mercado LM, Sitch S, *et al*. (2011) The Joint UK Land Environment Simulator (JULES), model description–Part 2: carbon fluxes and vegetation dynamics. *Geoscientific Model Development*, **4**, 701-722.

Collatz GJ, Ball JT, Grivet C, *et al*. (1991) Physiological and environmental regulation of stomatal conductance, photosynthesis and transpiration: a model that includes a laminar boundary layer. *Agricultural and Forest Meteorology*, **54**, 107-136.

Cox PM, Pearson D, Booth BB, *et al*. (2013) Sensitivity of tropical carbon to climate change constrained by carbon dioxide variability. *Nature*, **494**, 341-344.

Dai Y, Zeng X, Dickinson RE, *et al*. (2003) The common land model. *Bulletin of the American Meteorological Society*, **84**, 1013-1023.

de Gonçalves LG, Borak JS, Costa MH, *et al*. (2013) Overview of the large-scale biosphere–atmosphere experiment in Amazonia Data Model Intercomparison Project (LBA-DMIP). *Agricultural and Forest meteorology*, **182**, 111-127.

dePury DGG, Farquhar GD (1997) Simple scaling of photosynthesis from leaves to canopies without the errors of big-leaf models. *Plant, Cell & Environment*, **20**, 537-557.

de Weirdt M, Verbeeck H, Maignan F, *et al*. (2012) Seasonal leaf dynamics for tropical evergreen forests in a process-based global ecosystem model. *Geoscientific Model Development*, **5**, 1091–1108.

Doughty CE, Goulden ML (2008) Seasonal patterns of tropical forest leaf area index and CO2 exchange. *Journal of Geophysical Research-Biogeosciences*, **113**, G00B06, doi:10.1029/2007JG000590.

Drewry DT, Kumar P, Long S, *et al.* (2010) Ecohydrological responses of dense canopies to environmental variability: 1. Interplay between vertical structure and photosynthetic pathway.*Journal of Geophysical Research: Biogeosciences*, **115**, G04022, doi: 10.1029/2010JG001340.

Ellsworth DS, Reich PB **(**1993) Canopy structure and vertical patterns of photosynthesis and related leaf traits in a deciduous forest**.** *Oecologia,* **96**, 169-178.

Farquhar GD, von Caemmerer S, Berry JA (1980) A biochemical model of photosynthetic CO2 assimilation in leaves of C3 species. *Planta*, **149**, 78-90.

Fisher RA, Muszala S, Verteinstein M, *et al.* (2015) Taking off the training wheels: the properties of a dynamic vegetation model without climate envelopes. *Geosci. Model Dev. Discuss*, **8**, 3293-3357.

Friedlingstein P, Cox P, Betts R, *et al.* (2006) Climate-carbon cycle feedback analysis: Results from the C4MIP model intercomparison. *Journal of Climate*, **19**, 3337-3353.

Friedlingstein P, Meinshausen M, Arora VK, *et al.* (2014) Uncertainties in CMIP5 climate projections due to carbon cycle feedbacks. *Journal of Climate*, **27**, 511-526.

Fu R, Yin L, Li W, *et al.* (2013) Increased dry-season length over southern Amazonia in recent decades and its implication for future climate projection. *Proceedings of the National Academy of Sciences of the United States of America*, **110**, 18110–18115.

Girardin CA, Malhi Y, Doughty CE, *et al.* (2016) Seasonal trends of Amazonian rainforest phenology, net primary productivity, and carbon allocation. *Global Biogeochemical Cycles*, **30**, 700-715.

Guan K, Pan M, Li H, *et al.* (2015) Photosynthetic seasonality of global tropical forests constrained by hydroclimate. *Nature Geoscience*, ***8***, 284-289.

Harper A, Cox P, Friedlingstein P, *et al.* (2016) Improved representation of plant functional types and physiology in the Joint UK Land Environment Simulator (JULES v4. 2) using plant trait information. *Geoscientific Model Development Discussions*, doi:10.5194/gmd-2016-22

He L, Chen JM, Pisek J, *et al.* (2012) Global clumping index map derived from the MODIS BRDF product. *Remote Sensing of Environment*, **119**, 118-130.

Heskel MA, Atkin OK, Turnbull MH, Griffin KL (2013) Bringing the Kok effect to light: a review on the integration of daytime respiration and net ecosystem exchange. *Ecosphere*, **4**, 1-14.

Hutyra LR, Munger JW, Saleska SR, *et al.* (2007) Seasonal controls on the exchange of carbon and water in an Amazonian rain forest. *Journal of Geophysical Research: Biogeosciences*, **112**, G03008, doi: 10.1029/2006JG000365.

Huntingford C, Zelazowski P, Galbraith D, *et al.* (2013) Simulated resilience of tropical rainforests to CO2-induced climate change. *Nature Geoscience*, **6**, 268-273.

Kenzo T, Inoue Y, Yoshimura M, *et al.* (2015) Height-related changes in leaf photosynthetic traits in diverse Bornean tropical rain forest trees. *Oecologia*, **177**, 191-202.

731 Kim Y, Knox RG, Longo M, *et al.* (2012) Seasonal carbon dynamics and water fluxes in an
732 Amazon rainforest. *Global Change Biology*, **18**, 1322–1334.

733 Kitajima K, Mulkey S, Wright S. (1997a) Decline of photosynthetic capacity with leaf age in
734 relation to leaf longevities for five tropical canopy tree species. *American Journal of*
735 *Botany*, **84**, 702-702.

736 Kitajima K, Mulkey S, Wright S (1997b) Seasonal leaf phenotypes in the canopy of a tropical
737 dry forest: photosynthetic characteristics and associated traits. *Oecologia*, **109**, 490-498.

738 Kumagai T, Ichie T, Yoshimura M, *et al.* Modeling CO2 exchange over a Bornean tropical rain
739 forest using measured vertical and horizontal variations in leaf-level physiological
740 parameters and leaf area densities. *Journal of Geophysical Research: Atmospheres*, **111**,
741 D10107, doi:10.1029/2005JD006676.

742 Lee JE, Frankenberg C, van der Tol C, *et al.* (2013) Forest productivity and water stress in
743 Amazonia: observations from GOSAT chlorophyll fluorescence. *Proceedings of the Royal*
744 *Society of London B: Biological Sciences*, **280**, 20130171.

745 Lin YS, Medlyn BE, Duursma RA, *et al.* (2015) Optimal stomatal behaviour around the
746 world. *Nature Climate Change*, **5**, 459-464.

747 Lloyd J, Farquhar GD (2008) Effects of rising temperatures and [CO2] on the physiology of
748 tropical forest trees. *Philosophical Transactions of the Royal Society B: Biological*
749 *Sciences*, **363**, 1811-1817.

750 Lloyd J, Patino S, Paiva RQ, *et al.* (2010) Optimisation of photosynthetic carbon gain and
751 within-canopy gradients of associated foliar traits for Amazon forest trees. *Biogeosciences*,
752 **7**, 1833-1859.

753 Lopes AP, Nelson BW, Wu J, *et al.* (2016) Leaf flush drives dry season green-up of the Central
754 Amazon. *Remote Sensing of Environment*, **182**, 90-98.

755 Lowman MD (1992) Leaf growth dynamics and herbivory in five species of Australian rain-
756 forest canopy trees. *Journal of Ecology*, **80**, 433-447.

757 Malhado AC, Costa MH, de Lima FZ, *et al.* (2009) Seasonal leaf dynamics in an Amazonian
758 tropical forest. *Forest ecology and management*, **258**, 1161-1165.

759 Medlyn BE, Duursma RA, Eamus D, *et al.* (2011) Reconciling the optimal and empirical
760 approaches to modelling stomatal conductance. *Global Change Biology*, **17**, 2134-2144.

761 Medvigy D, Wofsy SC, Munger JW, *et al.* (2009) Mechanistic scaling of ecosystem function and
762 dynamics in space and time: Ecosystem Demography model version 2. *Journal of*
763 *Geophysical Research: Biogeosciences*, **114**, G01002, doi: 10.1029/2008JG000812.

764 Messier C, Parent S, and Bergeron Y. (1998) Effects of overstory and understory vegetation on
765 the understory light environment in mixed boreal forests. *Journal of Vegetation Science*, **9**,
766 511-520.

767 Messier J, McGill BJ, Enquist BJ, Lechowicz MJ. (2016) Trait variation and integration across
768 scales: Is the leaf economic spectrum present at local scales? *Ecography*,
769 10.1111/ecog.02006.

Miyaji K, Silva WS, Paulo TA (1997) Longevity of leaves of a tropical tree, Theobroma cacao, grown under shading, in relation to position within the canopy and time of emergence. *New Phytologist*, **135**, 445-454.

Morton DC, Nagol J, Carabajal CC, *et al.* (2014) Amazon forests maintain consistent canopy structure and greenness during the dry season. *Nature*, **506**, 221-224.

Morton DC, Rubio J, Cook BD, *et al.* (2016) Amazon forest structure generates diurnal and seasonal variability in light utilization. *Biogeosciences*, **13,** 2195-2206.

Myneni RB, Yang W, Nemani RR, *et al.* (2007) Large seasonal swings in leaf area of Amazon rainforests. *Proceedings of the National Academy of Sciences*, **104**, 4820-4823.

Niinemets Ü, Keenan TF, and Hallik L. (2015) A worldwide analysis of within-canopy variations in leaf structural, chemical and physiological traits across plant functional types. *New Phytologist*, **205**, 973-993.

Oleson KW, Lawrence DM, Bonan GB, *et al.* (2013) *Technical description of version 4.5 of the Community Land Model (CLM). NCAR Tech.* Note NCAR/TN-503+ STR. National Center for Atmospheric Research, Boulder, CO, 422 pp. doi: 10.5065/D6RR1W7M, 2013.

Pan Y, Birdsey RA, Fang J, *et al.* (2011) A large and persistent carbon sink in the world's forests." *Science*, **333**, 988-993.

Powell TL, Galbraith DR, Christoffersen BO, *et al.* (2013) Confronting model predictions of carbon fluxes with measurements of Amazon forests subjected to experimental drought. *New Phytologist*, **200**, 350–365.

Pyle EH, Santoni GW, Nascimento HE, *et al.* (2008) Dynamics of carbon, biomass, and structure in two Amazonian forests. *Journal of Geophysical Research: Biogeosciences*, **113**, G00B08, doi:10.1029/2007JG000592.

Reich PB, Uhl C, Walters MB, *et al.* (2004) Leaf demography and phenology in Amazonian rain forest: a census of 40 000 leaves of 23 tree species. *Ecological Monographs*, **74**, 3-23.

Restrepo-Coupe N, da Rocha HR, Hutyra LR, *et al.* (2013) What drives the seasonality of photosynthesis across the Amazon basin? A cross-site analysis of eddy flux tower measurements from the Brasil flux network. *Agricultural and Forest Meteorology*, **182**, 128–144.

Restrepo-Coupe N, Levine N, Christoffersen BO, *et al.* (2017) Do dynamic global vegetation models capture the seasonality of carbon fluxes in the Amazon basin? A data-model intercomparison. *Global Change Biology*, **23**, 191-208.

Rice AH, Pyle EH, Saleska SR, *et al.* (2004) Carbon balance and vegetation dynamics in an old-growth Amazonian forest. *Ecological Applications*, **14**, 55-71.

Richardson AD, Hollinger DY, Aber JD, *et al.* (2007) Environmental variation is directly responsible for short-but not long-term variation in forest-atmosphere carbon exchange. *Global Change Biology*, **13**, 788-803.

Richardson AD & O'Keefe J. (2009) Phenological differences between understory and overstory. In *Phenology of ecosystem processes* (pp. 87-117). Springer New York.

Richardson AD, Anderson RS, Arain MA, *et al.* (2012) Terrestrial biosphere models need better representation of vegetation phenology: results from the North American Carbon Program Site Synthesis. *Global Change Biology*, **18**, 566-584.

Roberts DA, Nelson BW, Adams JB, *et al.* (1998) Spectral changes with leaf aging in Amazon caatinga. *Trees*, **12**, 315-325.

Rogers A, Medlyn BE, Dukes JS, *et al.* (2017) A Roadmap for improving the representation of photosynthesis in Earth System Models. *New Phytologist*, **213**, 22-42.

Ryu Y, Baldocchi DD, Kobayashi H, *et al.* (2011) Integration of MODIS land and atmosphere products with a coupled-process model to estimate gross primary productivity and evapotranspiration from 1 km to global scales. *Global Biogeochemical Cycles*, **25**, GB4017, doi:10.1029/2011GB004053.

Saleska SR, Miller SD, Matross DM, *et al.* (2003) Carbon in Amazon forests: unexpected seasonal fluxes and disturbance-induced losses. Science, **302**, 1554–1557.

Saleska SR, Wu J, Guan K, *et al.* (2016) Brief Communications Arising: Dry season greening of Amazon forests. *Nature*, **531:** E4-E5.

Saatchi SS, Harris NL, Brown S, *et al.* (2011) Benchmark map of forest carbon stocks in tropical regions across three continents. *Proceedings of the National Academy of Sciences*, **108**, 9899-9904.

Schimel D, Pavlick R, Fisher JB, *et al.* (2015) Observing terrestrial ecosystems and the carbon cycle from space. *Global change biology*, **21**, 1762-1776.

Sellers PJ (1987) Canopy reflectance, photosynthesis, and transpiration, II. The role of biophysics in the linearity of their interdependence. *Remote sensing of Environment*, **21**, 143-183.

Sellers PJ, Berry JA, Collatz, *et al.* (1992) Canopy reflectance, photosynthesis, and transpiration. III. A reanalysis using improved leaf models and a new canopy integration scheme. *Remote sensing of environment*, **42**, 187-216.

Serbin SP, Singh A, Desai AR, *et al.* (2015) Remotely estimating photosynthetic capacity, and its response to temperature, in vegetation canopies using imaging spectroscopy. *Remote Sensing of Environment*, **167**, 78-87

Sitch S, Friedlingstein P, Gruber N, *et al.* (2015) Recent trends and drivers of regional sources and sinks of carbon dioxide. *Biogeosciences*, **12**, 653-679.

Stark SC, Leitold V, Wu JL, *et al.* (2012) Amazon forest carbon dynamics predicted by profiles of canopy leaf area and light environment. *Ecology letters*, **15**, 1406-1414.

Stark SC, Enquist BJ, Saleska SR, *et al.* (2015) Linking canopy leaf area and light environments with tree size distributions to explain Amazon forest demography. *Ecology letters*, **18**, 636-645.

Stark SC, Breshears DD, Garcia ES, *et al.* (2016) Toward accounting for ecoclimate teleconnections: intra-and inter-continental consequences of altered energy balance after vegetation change. *Landscape Ecology*, **31**, 181-194.

848 Wehr R, Munger JW, McManus JB, *et al*. (2016) Seasonality of temperate forest photosynthesis
849 and daytime respiration. *Nature*, **534**, 680-683.

850 Wright IJ, Leishman MR, Read C and Westoby M. (2006) Gradients of light availability and leaf
851 traits with leaf age and canopy position in 28 Australian shrubs and trees. *Functional Plant*
852 *Biology*, **33**, 407-419.

853 Wright SJ, Van Schaik CP (1994) Light and the phenology of tropical trees. *American*
854 *Naturalist,* **143**, 192-199.

855 Wu J, Albert LP, Lopes AP, Restrepo-Coupe N, *et al*. (2016a). Leaf development and
856 demography explain photosynthetic seasonality in Amazon evergreen forests." *Science*,
857 **351**, 972-976.

858 Wu J, Chavana-Bryant C, Prohaska N, *et al*. (2016b). Convergence in relationships between leaf
859 traits, spectra and age across diverse canopy environments and two contrasting tropical
860 forests. *New Phytologist*, doi:10.1111/nph.10451.

861 Wu J, Guan K, Hayek M, *et al.* (2017) Partitioning the extrinsic and intrinsic controls on gross
862 ecosystem productivity at hourly to inter-annual time scales in an Amazonian evergreen
863 forest. *Global Change Biology*, **3**, 1240-1257.

864 Xu X, Medvigy D, Powers JS, *et al*. (2016) Diversity in plant hydraulic traits explains seasonal
865 and inter-annual variations of vegetation dynamics in seasonally dry tropical forests. *New*
866 *Phytologist*, **212**, 80-95.

867
868

869 Main Figures and Tables

870 **Table 1.** Correlations between the seasonality of eddy covariance derived GPP_{ref} and the
871 seasonality of modeled GPP_{ref} using three different models parameterized by four different
872 inputs of leaf phenology. R^2 for coefficient of determination; p, or p-value, for significance of the
873 test; within-canopy phenological variation for the two-fraction leaf, two-layer canopy model was
874 parameterized when ftop=0.7; NA for not applicable.

Model\Phenology	Quantity	Quality	Quantity+Quality	Quantity+Quality+Within-Canopy Variation
DF1997	(R^2=0.19; p=0.041)	(R^2=0.69; p<0.0001)	(R^2=0.80; p<0.0001)	NA
ML	(R^2=0.17; p=0.042)	(R^2=0.72; p<0.0001)	(R^2=0.81; p<0.0001)	NA
Two-fraction leaf, two-layer canopy	(R^2=0.17; p=0.042)	(R^2=0.72; p<0.0001)	(R^2=0.81; p<0.0001)	(R^2=0.90; p<0.0001)

875

876 Caption for Main Figures

877 **Figure 1.** Mean annual cycles of monthly LAI in three age classes (three different color lines) at
878 the Tapajós k67 site (adapted from Fig. 3A in Wu *et al.*, 2016a). The three-age LAI seasonality
879 was modeled using the same leaf age residence time parameter as Wu *et al* (2016a), constrained
880 to sum to total camera-observed LAI (black squares) at the same forest site. Shading indicates
881 the dry season.

882 **Figure 2.** Vertical change in leaf level V_{cmax25} with cumulative LAI from canopy top to forest
883 floor, using the eqns. 5-6, following Lloyd *et al* (2010). Three color lines represent leaves at
884 three age classes (Young: 1-2 months; Mature: 3-5 months; Old: ≥6 months) respectively.
885 V_{cmax25} of three age classes at the top of the canopy are derived from leaf level gas exchange
886 measurements at the Tapajós k67 site (n=5 tree species; also see Wu *et al.*, 2016a).

887 **Figure 3.** Seasonal variation in EC-derived GPP_{ref} (seven-year mean annual cycle; black
888 squares) and modeled GPP_{ref} (grey circles) incorporating different phenological components,
889 using the two-fraction leaf, two-layer canopy model. (a) modeled GPP_{ref} parameterized by
890 seasonal variation in leaf quantity (or LAI) only; (b) modeled GPP_{ref} parameterized by seasonal
891 variation in both leaf quantity and quality, while assuming a constant leaf turnover rate
892 throughout the vertical canopy profile; (c) modeled GPP_{ref} parameterized by seasonal variation in
893 leaf quantity and quality, and differential leaf turnover rates within a forest canopy (i.e.
894 ftop=0.7). Shading indicates the dry season; ftop refers to the fraction of observed leaf turnover
895 across the whole forest canopy attributed to leaves in the upper canopy layer.

896 **Figure 4.** Differential photosynthetic sensitivity of the canopy sunlit fraction and the canopy
897 shade fraction to seasonal variation in leaf quantity (Fig. 1) and leaf quality (Fig. 1 and eqn. 1) at
898 the Tapajós k67 site assessed by using the two-fraction leaf, two-layer canopy model under the
899 reference environment: (a) canopy absorbed PAR, (b) canopy LAI, (c) canopy integrated V_{cmax},
900 and (d) canopy GPP_{ref}. Data are shown for total canopy (black circles), the sunlit canopy fraction
901 (black triangles) and the shaded canopy fraction (grey triangles); canopy-scale V_{cmax} (of per-
902 ground area) is the sum of canopy LAI weighted by leaf level V_{cmax} (see Table S3 for equations),
903 and since the LAI of the shade canopy fraction is higher than the LAI of the sunlit canopy
904 fraction, as such V_{cmax} of the shade canopy fraction is higher than V_{cmax} of the sunlit canopy
905 fraction; shading indicates the dry season.

906 **Figure 5.** Assessing the effect of within-canopy phenological variation (i.e. ftop) on canopy
907 photosynthetic seasonality using the two-fraction leaf, two-layer canopy model. (a) Modeled
908 annual cycles of GPP_{ref} (relative to annual maxima) under different ftop values from 0.2 to 1.0;
909 and (b) R^2 between modeled and EC-derived GPP_{ref} seasonality plotted against ftop. Shading
910 indicates dry season; ftop refers to the fraction of observed leaf turnover across the whole forest
911 canopy attributed to leaves in the upper canopy layer.

912

913 Caption for Supplementary Figures and Supplementary Tables

914 **Figure S1.** The sensitivity of modeled canopy-scale GPP using the multi-layer model (ML) to
915 the number of layers used for model simulation, under (a) highly cloudy environment ($PAR_{b,0}$=10.1 μmol m^{-2} s^{-1} vs. $PAR_{d,0}$=260.3 μmol m^{-2} s^{-1}), (b) intermediate cloudy environment
917 ($PAR_{b,0}$=743.9 μmol m^{-2} s^{-1}vs. $PAR_{d,0}$=268. μmol m^{-2} s^{-1}), and (c) clear sky environment
918 ($PAR_{b,0}$=1850.5 μmol m^{-2} s^{-1} vs. $PAR_{d,0}$=173.7 μmol m^{-2} s^{-1}). For model simulation, $PAR_{b,0}$ for
919 canopy surface direct beam and $PAR_{d,0}$ for canopy surface diffuse beam; solar zenith angle=30°,
920 LAI=6 m^2m^{-2}, leaf temperature=28°C; ambient CO_2 concentration=380 ppm; V_{cmax25}=40 μmol
921 CO_2 m^{-2} s^{-1}.
922
923 **Figure S2.** The sensitivity analysis of LAI cutoff (which divides the canopy into upper and lower
924 canopy layers) on modeled canopy-scale GPP_{ref} seasonality parameterized by field derived leaf
925 quantity and quality by using the two-fraction leaf, two-layer canopy model under three different
926 ftop values: (a) ftop=0.4, (b) ftop=0.6, and (c) ftop=0.8. Three color lines represent different LAI
927 cutoff. Shading indicates the dry season.

928 **Figure S3.** Cross model comparisons for canopy-scale GPP-PAR relationship between DF1997
929 (red line) and ML (black line). For model simulation, solar zenith angle=30°, LAI=6 m^2m^{-2}, leaf
930 temperature=28°C; ambient CO_2 concentration=380 ppm; V_{cmax25}=40 μmol CO_2 m^{-2} s^{-1}.
931
932 **Figure S4.** Average annual cycle of modeled FAPAR (relative to annual maxima) using the two-
933 fraction leaf, two-layer canopy model at the Tapajós k67 site under three scenarios: whole
934 canopy (black circles), the sunlit canopy fraction (black triangles), and the shade canopy fraction
935 (grey triangles). Shading indicates the dry season.
936
937 **Figure S5.** GPP-PAR relationship simulated by the FvCB model under each given V_{cmax25} (in
938 μmol CO_2 m^2 s^{-1}; represented as different color lines).

939 **Figure S6.** Average annual cycle of GPP_{ref} (relative to annual maxima) at the Tapajós k67 site
940 under four scenarios: eddy covariance derived GPP_{ref} (red line), and modeled GPP_{ref} by using the
941 two-fraction leaf, two-layer canopy model for the whole canopy (black circles), for the canopy of
942 sunlit fraction (black triangles), and for the canopy of shade fraction (grey triangles). Shading
943 indicates the dry season.
944

Table S1. Individual canopy trees for leaf gas exchange measurements of top-of-canopy sunlit leaves in 2012 campaign at the Tapajós k67 site (adapted from Wu *et al.*, 2016a). Species represented by these individuals account for 23.7% of basal area of vegetative community at the k67 site. NA for not applicable.

Scientific name	Family	Maximum canopy height (m)	Basal area abundance	Leaf age class	Number of leaves	V_{cmax25} (μmol CO_2 m^{-2} s^{-1})
Erisma uncinatum Warm.	Vochysiaceae	40	10.1%	Young	3	15.1
				Mature	3	26.3
				Old	3	21.1
Chamaecrista scleroxylon (Ducke) H.S.Irwin & BarnebyChamaecrista xinguensis	Leguminosae-Caesalpinioideae	27	4.47%	Young	1	11.2
				Mature	1	35.8
				Old	1	17.9
Manilkara huberi (Ducke) A.Chev.	Sapotaceae	37	6.54%	Young	1	13.7
				Mature	1	34.6
				Old	1	33.0
Tachigali eriopetala (Ducke) L.G.Silva & H.C.Lima	Leguminosae-Caesalpinioideae	44	1.55%	Young	2	14.0
				Mature	2	56.7
				Old	2	23.2
Ocotea sp.	Lauraceae	38	1.06%	Young	NA	NA
				Mature	2	29.0
				Old	4	21.4

Table S2. Modified equations of the Farquhar, von Caemmerer and Berry (FvCB; Farquhar *et al.*, 1980) leaf photosynthesis model, coupled with Medlyn type stomatal conductance scheme (Medlyn *et al.*, 2011). Symbols of constant are defined in Table S6, and values of the Rubisco parameters are given in Table S7.

Equations	Definition	No.	Ref.
$GPP_l = \min\{A_v, A_j, A_s\} - R_l$	Leaf level gross primary productivity (GPP, μmol CO_2 m^{-2} s^{-1})	1	A
$A_v = \max\{V_{c\max} \times \frac{C_i - \Gamma_*}{C_i + K'}, 0\}$	Rubisco-limited photosynthesis (μmol CO_2 m^{-2} s^{-1})	2	A
$K' = K_C \times (1 + \frac{O}{K_O})$	Effective Michaelis-Menten Constant	3	A
$A_j = \max\{J \times \frac{C_i - \Gamma_*}{4 \times (C_i + 2 \times \Gamma_*)}, 0\}$	Electron-transport limited rate of photosynthesis (μmol CO_2 m^{-2} s^{-1})	4	A
$J_e = \Phi_{PSII,\max} \times \alpha \times \beta \times Q$	The rate of whole electron transport (μmol m^{-2} s^{-1})	5	C
$J = \frac{J_e + J_{\max} - \sqrt{(J_e + J_{\max})^2 - 4 \times \Theta \times J_e \times J_{\max}}}{2 \times \Theta}$	The rate of electrons through the thylakoid membrane (μmol CO_2 m^{-2} s^{-1})	6	A
$A_s = 0.5 \times V_{c\max}$	Triose phosphate export limited rate of photosynthesis (μmol CO_2 m^{-2} s^{-1})	7	B
$Parameter = Parameter_{25} \times \exp(\frac{(T_K - 298) \times \Delta H_a}{R \times T_K \times 298})$	Temperature functions for parameters that are based on Rubisco kinetic properties and do not have an optimum within a biologically significant temperature range (K_C, K_O, Γ_*, R_l, and in most cases $V_{c\max 25}$)	8	C
$J_{\max} = J_{\max 25} \times \frac{e^{-(\frac{T_L - T_{opt}}{\Omega_T})}}{e^{-(\frac{25 - T_{opt}}{\Omega_T})}}$	Temperature function for maximum electron transport rate, J_{max}	9	C, D
$\Omega_T = 11.6 + 0.18 \times T_{opt}$	Coefficient for temperature function of J_{max}	10	C, D
$J_{\max 25} = 1.67 \times V_{c\max 25}$	Linear scaling relationship between $J_{\max 25}$ and $V_{c\max 25}$	11	E, F
$T_K = T_l + 273.15$	Leaf temperature in Kelvin	12	C
$R_{l25} = 0.015 \times V_{c\max 25}$	Leaf dark respiration at 25°C (μmol CO_2 m^{-2} s^{-1})	13	E
$g_s = 1.6 \times (1 + \frac{g_1}{\sqrt{VPD}}) \times \frac{GPP_l}{C_a}$ $GPP_l = g_s \times (C_a - C_i)$ $\Rightarrow C_i = C_a \times (1 - \frac{1}{1.6 \times (1 + \frac{g_1}{\sqrt{VPD}})})$	Use optimal stomatal model to estimate internal CO_2 concentration (C_i) from atmospheric CO_2 concentration (C_a) and vapor pressure deficit (VPD)	14	G

A: Farquhar *et al.*, 1980; B: Ryu *et al.*, 2011; C: Bernacchi *et al.*, 2013; D: June *et al.*, 2004; E: Bonan *et al.*, 2014; F: Medlyn *et al.*, 2002; G: Medlyn *et al.*, 2011.

Table S3. Modified equations of V_{cmax} for the canopy of sunlit and shade fractions. Symbols of constant are defined in Table S6, and values of the Rubisco parameters are given in Table S7.

Equations	Definition	No.	Ref.
$V_{cmax,tot} = \frac{V_{cmax,0}}{k_n} \times (1 - \exp^{(-k_n \times LAI_{tot})})$	Canopy total V_{cmax} (μmol CO_2 m^{-2} s^{-1})	15	A
$V_{cmax,sun} = \frac{V_{cmax,0} \times \Omega}{k_n + k_b \times \Omega} \times (1 - \exp^{(-(k_n + k_b \times \Omega) \times LAI_{tot})})$	V_{cmax} for the canopy of sunlit cohort (μmol CO_2 m^{-2} s^{-1})	16	A, B
$V_{cmax,shade} = V_{cmax,tot} - V_{cmax,sun}$	V_{cmax} for the canopy of shade cohort (μmol CO_2 m^{-2} s^{-1})	17	A, B
$k_n = \exp^{(0.00963 \times V_{cmax,0} - 2.43)}$	Coefficient of V_{cmax} decline within a forest canopy	18	H
$k_b = \frac{0.5}{\cos(SZA)}$	Beam radiation extinction coefficient of the canopy	19	A

A: Farquhar *et al.*, 1980; B: Ryu *et al.*, 2011; H: Lloyd *et al.*, 2010.

Table S4. Modified equations of absorbed photosynthetically active radiation (PAR) by the canopy of sunlit and shade fractions. Symbols of constant are defined in Table S6, and values of the Rubisco parameters are given in Table S7.

Equations	Definition	No.	Ref.
$Q_{tot} = (1-\rho_{cb}) \times PAR_{b,0} \times (1-\exp^{-k_b^{'} \times LAI_{tot} \times \Omega}) + (1-\rho_{cd}) \times PAR_{d,0} \times (1-\exp^{-k_d^{'} \times LAI_{tot} \times \Omega})$	Canopy absorbed total radiation (μmol m^{-2} s^{-1})	20	A, B
$Q_{b,sun} = PAR_{b,0} \times (1-\sigma) \times (1-\exp^{-k_b \times LAI_{tot} \times \Omega})$	The absorbed incoming beam radiation by sunlit leaves (μmol m^{-2} s^{-1})	21	A, B
$Q_{d,sun} = PAR_{d,0} \times (1-\rho_{cd}) \times (1-\exp^{-(k_d^{'}+k_b) \times LAI_{tot} \times \Omega})$	The absorbed incoming diffuse radiation by sunlit leaves (μmol m^{-2} s^{-1})	22	A, B
$Q_{s,sun} = PAR_{b,0} \times [(1-\rho_{cb}) \times (1-\exp^{-(k_b^{'}+k_b) \times LAI_{tot} \times \Omega}) \times \frac{k_b^{'}}{k_b^{'}+k_b} - (1-\sigma) \times (1-\exp^{-2 \times k_b \times LAI_{tot} \times \Omega}) \times \frac{1}{2}]$	The absorbed incoming scattered radiation by sunlit leaves (μmol m^{-2} s^{-1})	23	A, B
$Q_{sun} = Q_{b,sun} + Q_{d,sun} + Q_{s,sun}$	Canopy absorbed total radiation for sunlit leaves (μmol m^{-2} s^{-1})	24	A, B
$Q_{shade} = Q_{tot} - Q_{sun}$	Canopy absorbed total radiation for shade leaves (μmol m^{-2} s^{-1})	25	A, B
$k_b^{'} = \frac{0.46}{\cos(SZA)}$	Beam and scattered beam radiation extinction coefficient	26	A
$k_d^{'} = 0.719$	Diffuse and scattered diffuse radiation extinction coefficient	27	A

A: Farquhar *et al.*, 1980; B: Ryu *et al.*, 2011.

Table S5. Equations to calculate incoming photosynthetically active radiation (PAR) over a canopy. R_{short} denotes total short-wave radiations from in-situ observations. P denotes observed air pressure and P_0 denotes standard air pressure.

Equations	Definition	No.	Ref.
$R_{b,vis} = \frac{600 \times e^{-0.185 \times \frac{P}{P_0} \times m}}{m}$	Expected beam visible radiation under clear sky (W m^{-2})	28	N
$R_{d,vis} = \frac{0.4 \times (600 - R_{b,vis} \times m)}{m}$	Expected diffuse visible radiation under clear sky (W m^{-2})	29	N
$R_{b,nir} = \frac{720 \times e^{-0.06 \times \frac{P}{P_0} \times m} - w}{m}$	Expected diffuse visible radiation under clear sky (W m^{-2})	30	N
$R_{b,nir} = \frac{720 \times e^{-0.06 \times \frac{P}{P_0} \times m} - w}{m}$	Expected diffuse near-infrared radiation under clear sky (W m^{-2})	31	N
$f_{PAR} = \frac{R_{b,vis} + R_{d,vis}}{R_{b,nir} + R_{d,nir} + R_{b,vis} + R_{d,vis}}$	The fraction of total PAR over total incoming radiation (f_{PAR})	32	N
$f_{PAR,b} = \frac{R_{b,vis}}{R_{b,vis} + R_{d,vis}} \times (1 - (\frac{0.9 - \frac{R_{short}}{R_{b,nir} + R_{d,nir} + R_{b,vis} + R_{d,vis}}}{0.7})^2)$	The fraction of beam PAR over total PAR ($f_{PAR,b}$)	33	N
$PAR_{b,0} = R_{short} \times f_{PAR} \times f_{PAR,b}$	The canopy top photosynthetically active radiation in beam light ($PAR_{b,0}$)	34	N
$PAR_{d,0} = R_{short} \times f_{PAR} \times (1 - f_{PAR,b})$	The canopy top photosynthetically active radiation in diffuse ($PAR_{d,0}$) light	35	N
$w = 1320 \times 10^{-1.195 + 0.4459 \times \log_{10} m - 0.0345 \times (\log_{10} m)^2}$	Expected water absorbance of near-infrared radiation in the atmosphere (W m^{-2})	36	N
$m = \cos(SZA)^{-1}$	Parameter calculated from solar zenith angle (SZA)	37	N

N: Weiss & Norman, 1985.

Table S6. Table of constants used in leaf and canopy level photosynthesis model.

Symbols	Definition	Values	Ref.
C_i	Inter-celluar CO_2 concentration (=0.7*ambient CO_2 concentration; μmol mol^{-1})	266	A
O	Oxygen concentration (mmol mol^{-1})	205	A
α	Leaf absorbance	0.85	A, C
β	Fraction of photosystem II to photosystem I	0.5	A, C
$\Phi_{PSII,\max}$	Maximum quantum efficiency of PSII photochemistry	0.7	C
Θ	Curvature term	0.7	A, E
R	Universal gas constant (J mol^{-1} K^{-1})	8.314	A
$V_{c\max 25}$	Maximal carboxylation rate at 25°C (μmol/m^2/s)	Observation	K
T_{opt}	Optimal leaf temperature for J_{max} (°C)	35	I
$V_{c\max,0}$	Maximal carboxylation rate for leaves at canopy surface (μmol CO_2 m^{-2} s^{-1})	Observation	K
Ω	Clumping index	0.66	J
LAI_{tot}	Canopy total leaf area index (m^2/ m^2)	Observation	K
ρ_{cb}	Canopy reflection coefficient for beam radiation	0.029	A
ρ_{cd}	Canopy reflection coefficient for diffuse radiation	0.036	A
σ	Leaf scatting coefficient of radiation	0.15	A
g1	Slope for stomatal conductance model	3.77	L

A: Farquhar *et al.*, 1980; C: Bernacchi *et al.*, 2013; E: *Bonan et al.*, 2014; I: Lloyd & Farquhar, 2008; J: He *et al.*, 2005; K: Wu *et al.*, 2016a; L: Lin *et al.*, 2015.

982 **Table S7.** The values for c and ΔH_a (activation energy) describing the temperature response of
983 the five parameters used to predict CO_2 uptake by leaves during Rubisco-limited photosynthesis
984 in leaf level FvCB model (see Table S4) (reference: M: Bernacchi *et al*., 2001).
985

Parameter	Value at 25°C	c (dimensionless)	ΔH_a (kJ mol^{-1})
R_l (μmol/m^2/s)	R_{l25}	18.72	46.39
$V_{c\max}$ (μmol/m^2/s)	$V_{c\max 25}$	26.35	65.33
Γ_* (μmol/m^2/s)	42.75	19.02	37.83
K_C (μmol/m^2/s)	404.9	38.05	79.43
K_O (mmol/m^2/s)	278.4	20.30	36.38

986
987
988

989 **References**

990 [A] Farquhar GD, von Caemmerer S, Berry JA (1980) A biochemical model of photosynthetic
991 CO2 assimilation in leaves of C3 species. *Planta*, **149**, 78-90.

992 [B] Ryu Y, Baldocchi DD, Kobayashi H, *et al.* (2011) Integration of MODIS land and
993 atmosphere products with a coupled-process model to estimate gross primary productivity
994 and evapotranspiration from 1 km to global scales. *Global Biogeochemical Cycles*, **25**,
995 GB4017, doi:10.1029/2011GB004053.

996 [C] Bernacchi CJ, Bagley JE, Serbin SP, *et al.* (2010) Modelling C3 photosynthesis from the
997 chloroplast to the ecosystem. *Plant, cell & environment*, **36**, 1641-1657.

998 [D] June T, Evans JR, Farquhar GD. (2004) A simple new equation for the reversible
999 temperature dependence of photosynthetic electron transport: a study on soybean
1000 leaf. *Functional plant biology*, **31**, 275-283.

1001 [E] Bonan GB, Williams M, Fisher RA, *et al.* (2014) Modeling stomatal conductance in the earth
1002 system: linking leaf water-use efficiency and water transport along the soil–plant–
1003 atmosphere continuum. *Geoscientific Model Development*, **7**, 2193-2222.

1004 [F] Medlyn BE, Dreyer E, Ellsworth D, *et al.* (2002) Temperature response of parameters of a
1005 biochemically based model of photosynthesis. II. A review of experimental data. *Plant, Cell*
1006 *& Environment*, **25**, 1167-1179.

1007 [G] Medlyn BE, Duursma RA, Eamus D, *et al.* (2011) Reconciling the optimal and empirical
1008 approaches to modelling stomatal conductance. *Global Change Biology*, **17**, 2134-2144.

1009 [H] Lloyd J, Patino S, Paiva RQ, *et al.* (2010) Optimisation of photosynthetic carbon gain and
1010 within-canopy gradients of associated foliar traits for Amazon forest trees. *Biogeosciences*,
1011 **7**, 1833-1859.

1012 [I] Lloyd J, Farquhar GD (2008) Effects of rising temperatures and [CO2] on the physiology of
1013 tropical forest trees. *Philosophical Transactions of the Royal Society B: Biological*
1014 *Sciences*, **363**, 1811-1817.

1015 [J] He L, Chen JM, Pisek J, *et al.* (2012) Global clumping index map derived from the MODIS
1016 BRDF product. *Remote Sensing of Environment*, **119**, 118-130.

1017 [K] Wu J, Albert LP, Lopes AP, Restrepo-Coupe N, Hayek M, Wiedemann KT, Guan K, *et al.*
1018 (2016a). Leaf development and demography explain photosynthetic seasonality in Amazon
1019 evergreen forests." *Science*, **351**, 972-976.

1020 [L] Lin YS, Medlyn BE, Duursma RA, *et al.* (2015) Optimal stomatal behaviour around the
1021 world. *Nature Climate Change*, **5**, 459-464.

1022 [M] Bernacchi CJ, Singsaas EL, Pimentel C, A *et al.* (2001) Improved temperature response
1023 functions for models of Rubisco-limited photosynthesis. *Plant, Cell & Environment*, **24**,
1024 253-259.

1025 [N] Weiss, A., and J. M. Norman. 1985. Partitioning solar radiation into direct and diffuse,
1026 visible and near-infrared components. *Agricultural and Forest Meteorology*, **34**, 205–213.

1027

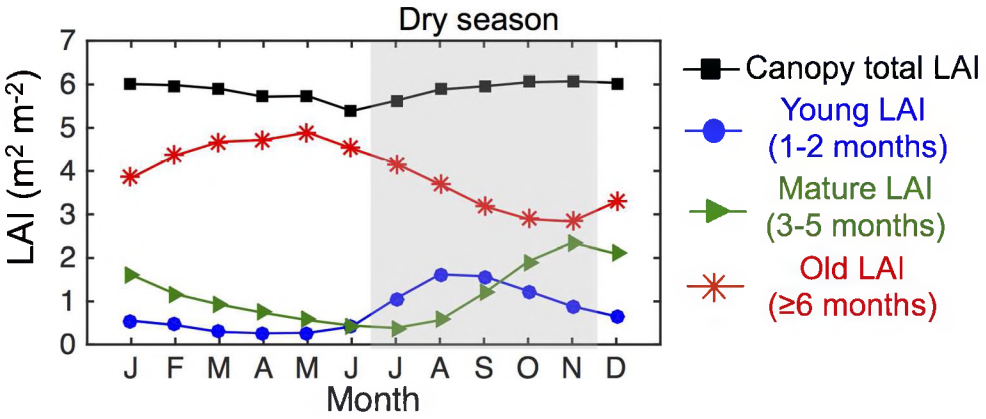

Figure 1. Mean annual cycles of monthly LAI in three age classes (three different color lines) at the Tapajós k67 site (adapted from Fig. 3A in Wu et al., 2016a). The three-age LAI seasonality was modeled using the same leaf age residence time parameter as Wu et al (2016a), constrained to sum to total camera-observed LAI (black squares) at the same forest site. Shading indicates the dry season.

144x62mm (300 x 300 DPI)

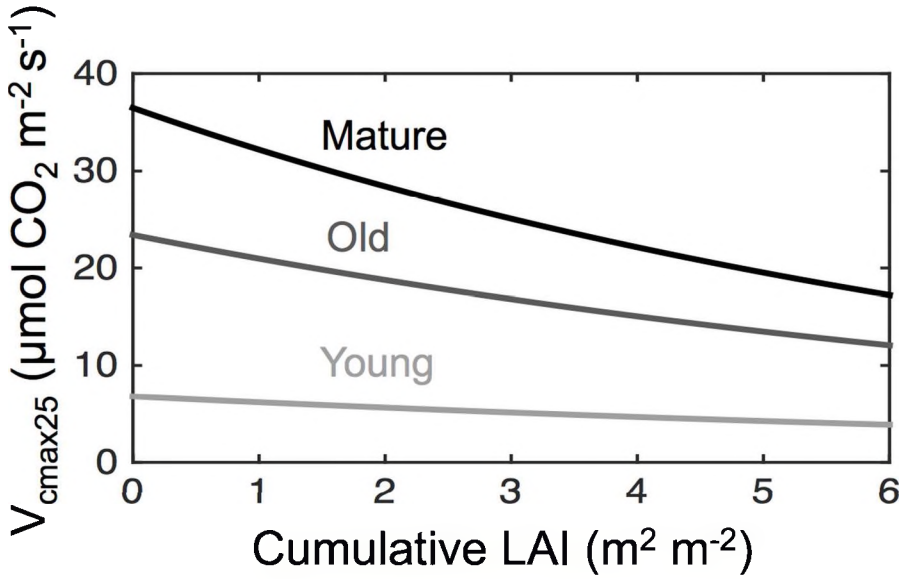

Figure 2. Vertical change in leaf level Vcmax25 with cumulative LAI from canopy top to forest floor, using the eqns. 5-6, following Lloyd et al (2010). Three color lines represent leaves at three age classes (Young: 1-2 months; Mature: 3-5 months; Old: ≥6 months) respectively. Vcmax25 of three age classes at the top of the canopy are derived from leaf level gas exchange measurements at the Tapajós k67 site (n=5 tree species; also see Wu et al., 2016a).

112x65mm (300 x 300 DPI)

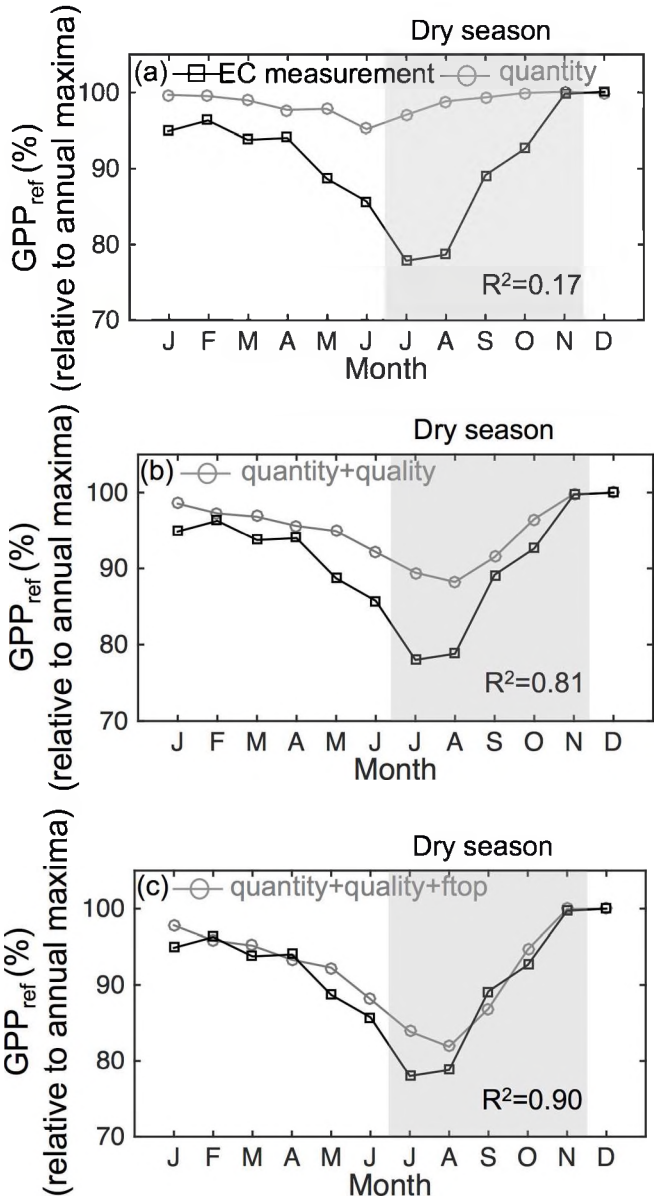

Figure 3. Seasonal variation in EC-derived GPPref (seven-year mean annual cycle; black squares) and modeled GPPref (grey circles) incorporating different phenological components, using the two-fraction leaf, two-layer canopy model. (a) modeled GPPref parameterized by seasonal variation in leaf quantity (or LAI) only; (b) modeled GPPref parameterized by seasonal variation in both leaf quantity and quality, while assuming a constant leaf turnover rate throughout the vertical canopy profile; (c) modeled GPPref parameterized by seasonal variation in leaf quantity and quality, and differential leaf turnover rates within a forest canopy (i.e. ftop=0.7). Shading indicates the dry season; ftop refers to the fraction of observed leaf turnover across the whole forest canopy attributed to leaves in the upper canopy layer.

120x197mm (300 x 300 DPI)

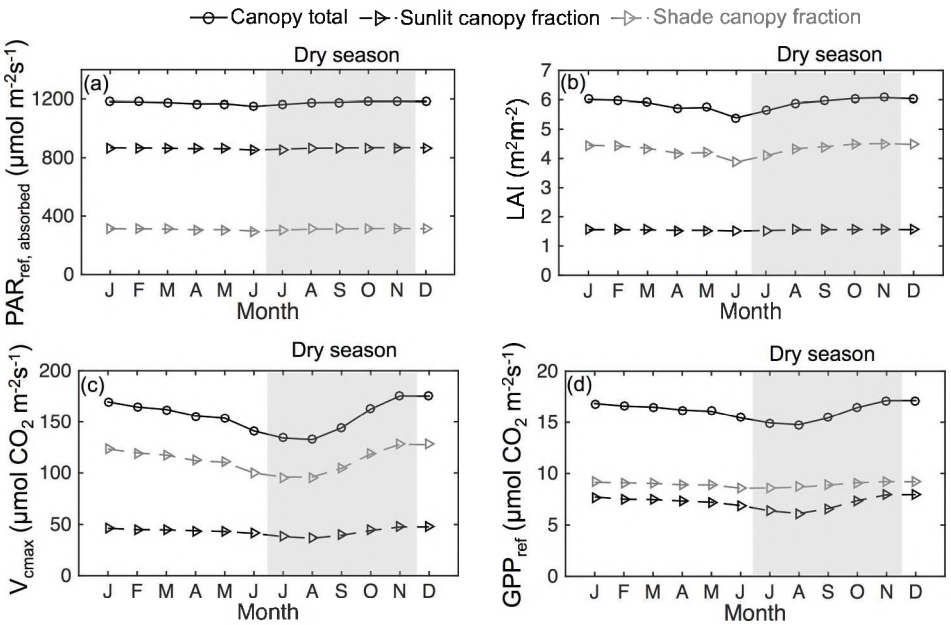

Figure 4. Differential photosynthetic sensitivity of the canopy sunlit fraction and the canopy shade fraction to seasonal variation in leaf quantity (Fig. 1) and leaf quality (Fig. 1 and eqn. 1) at the Tapajós k67 site assessed by using the two-fraction leaf, two-layer canopy model under the reference environment: (a) canopy absorbed PAR, (b) canopy LAI, (c) canopy integrated Vcmax, and (d) canopy GPPref. Data are shown for total canopy (black circles), the sunlit canopy fraction (black triangles) and the shaded canopy fraction (grey triangles); canopy-scale Vcmax (of per-ground area) is the sum of canopy LAI weighted by leaf level Vcmax (see Table S3 for equations), and since the LAI of the shade canopy fraction is higher than the LAI of the sunlit canopy fraction, as such Vcmax of the shade canopy fraction is higher than Vcmax of the sunlit canopy fraction; shading indicates the dry season.

219x137mm (300 x 300 DPI)

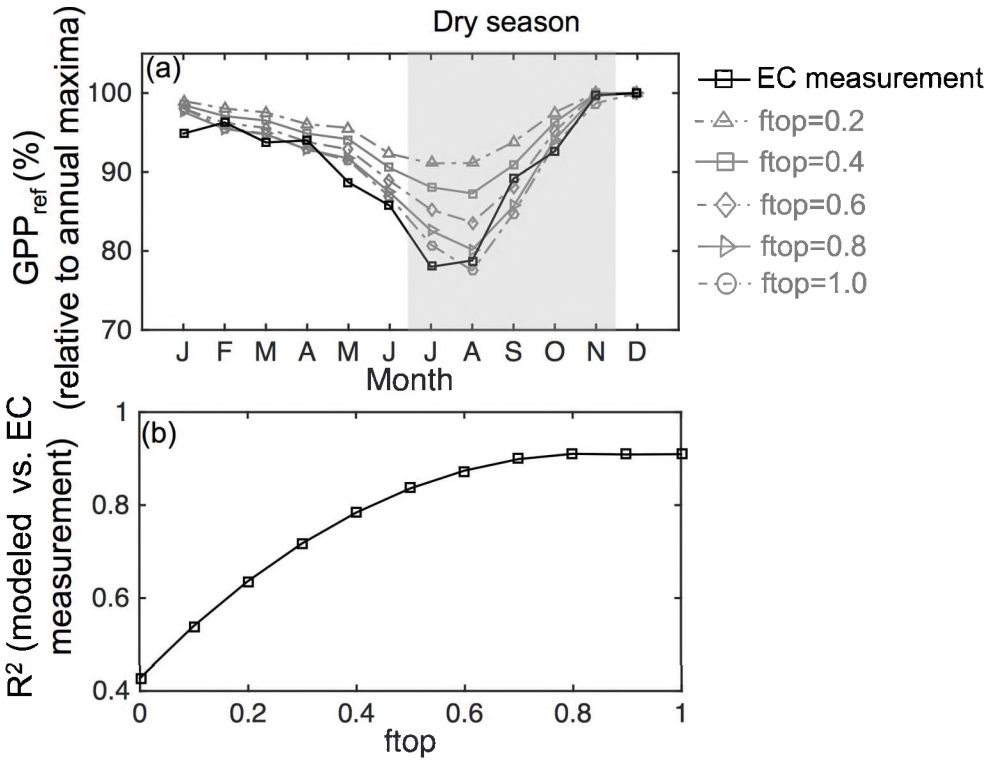

Figure 5. Assessing the effect of within-canopy phenological variation (i.e. ftop) on canopy photosynthetic seasonality using the two-fraction leaf, two-layer canopy model. (a) Modeled annual cycles of GPPref (relative to annual maxima) under different ftop values from 0.2 to 1.0; and (b) R2 between modeled and EC-derived GPPref seasonality plotted against ftop. Shading indicates dry season; ftop refers to the fraction of observed leaf turnover across the whole forest canopy attributed to leaves in the upper canopy layer.

157x120mm (300 x 300 DPI)